Unified Electromagnetic Theory of Matter and Light

Section D — **Structure and Dynamics of the Universe**

Part D2 - **Gamma-Ray Source**

Franc Rozman

Abstract

This study investigates an alternative interpretation of gamma-ray bursts (GRBs) as temporal concentrations of electromagnetic radiation emitted over substantially longer intervals. Rather than requiring a short-lived increase in intrinsic source luminosity, the proposed mechanism attributes the observed burst to a nonuniform mapping between emission and arrival times.

The model considers localized gamma-emitting regions within magnetized plasma or other high-energy astronomical environments. Their radial motion may be governed by the combined effects of gravitational, electromagnetic, and other forces. The arrival-time calculation adopts the source-dependent propagation hypothesis developed in Part C2, under which the effective propagation velocity relative to the observer depends on the radial motion of the emitting region. A temporal caustic occurs when the derivative of arrival time with respect to emission time approaches zero.

Gravitationally determined binary trajectories provide three quantitative examples in which emission lasting one hour, one day, or thirty days is mapped into observed intervals of a few seconds. In the thirty-day example, the mean temporal concentration factor is 864,000. The analysis examines pulse profiles, multiple arrival-time branches, finite emitting-region effects, and the integral energy balance. Local electromagnetic coherence and possible structural merging, considered in Part B2, may influence the uniformity of outgoing propagation characteristics, but are not assumed to have been quantitatively established.

The resulting framework predicts enhanced received power through temporal redistribution without creating electromagnetic energy within an ideal loss-free beam. Its applicability to observed GRBs remains conditional on independent tests of the propagation hypothesis, the physical realization of sufficiently synchronized emission, and an adequate source energy budget.

1. Introduction

Gamma-ray bursts (GRBs) are among the most intense transient electromagnetic phenomena observed in the Universe. Their radiation may reach extraordinary peak intensities within intervals ranging from fractions of a second to several minutes. Understanding these events requires explaining not only the production of high-energy electromagnetic radiation, but also the observed duration, intensity, temporal structure, and spectral evolution of the received signal.

Conventional interpretations associate GRBs primarily with energetic astrophysical processes, including the collapse of massive stars, mergers of compact objects, and relativistic outflows. In these models, the short duration and high luminosity of the observed event are related to rapid energy release and the dynamics of the emitting system.

The present study investigates a different possibility: **the observed duration of a gamma-ray burst need not correspond to the duration of electromagnetic emission at its source.**

An astronomical region may emit gamma radiation continuously over an extended interval, while the motion of the emitting region changes the propagation times of successive electromagnetic waves. Under suitable conditions, radiation emitted over hours, days, or longer intervals may reach a distant observer within only a few seconds.

The resulting gamma-ray burst would then represent a temporal concentration of previously emitted electromagnetic energy rather than necessarily requiring a sudden increase in the intrinsic luminosity of the source.

The proposed mechanism is based on the source-dependent propagation hypothesis developed in Part C2 of this research programme. According to this hypothesis, the propagation velocity of an electromagnetic wave relative to the observer depends on the radial velocity of its emitting source.

Consequently, changes in the radial velocity of the source may produce differences in the propagation times of electromagnetic waves emitted at successive instants.

When the derivative of the arrival time with respect to emission time approaches zero, electromagnetic radiation emitted over an extended interval becomes concentrated into a much shorter observational interval. This condition defines a temporal caustic and provides the mathematical foundation of the present GRB model.

A central question is whether such a critical condition can arise from physically determined astronomical motion rather than from an arbitrarily prescribed velocity or acceleration history.

The present study considers localized gamma-emitting regions within larger astronomical environments. Such regions may be associated with magnetized plasma surrounding compact objects, gravitationally interacting stellar systems, or other high-energy electromagnetic environments.

A neutron star may provide an important energy reservoir or gravitational component of such a system, but the proposed mechanism does not require the gamma radiation to originate directly from the stellar surface.

The emitting region is treated as the dynamical source whose radial velocity and acceleration influence the arrival-time distribution of the radiation.

Its motion may result from gravitational attraction, electromagnetic forces, pressure gradients, or combinations of these interactions. The decisive quantity is the resultant radial acceleration, rather than the magnitude of any individual force.

Gravitationally bound binary systems provide particularly useful quantitative examples because their orbital motion can be calculated directly from the masses, separation, and viewing geometry. The present study therefore retains gravitational binary trajectories as a means of testing whether the required

acceleration and its time variation can arise naturally.

The electromagnetic properties of the emitting region are also relevant.

A large magnetized plasma environment may contain many radiating structures with different positions and velocities. Radiation contributing to a sharply concentrated observed burst must therefore possess sufficiently compatible propagation histories.

Part B2 examines the proposed structural merging of compatible electromagnetic waves and coherent wave chains. Such interactions may contribute to the local adjustment of electromagnetic propagation characteristics before the radiation begins its long-distance propagation toward the observer.

The present article does not attempt to derive this microscopic merging mechanism. Instead, it considers the arrival-time consequences of radiation that has acquired sufficiently well-defined effective propagation characteristics.

The quantitative analysis develops examples in which emission lasting one hour, one day, or thirty days is concentrated into observational intervals of a few seconds under the assumed propagation relation.

The model also examines the resulting temporal intensity profiles, the possibility of multiple maxima, the influence of finite emitting-region dimensions, and the conservation of electromagnetic energy during temporal concentration.

In addition, the study considers how radiation from different regions of an extended astronomical environment may contribute to spectral evolution and broader electromagnetic emission preceding or following the principal gamma-ray maximum.

An essential distinction is maintained between the energy required to generate gamma radiation and the propagation conditions responsible for concentrating that radiation in observer time.

Temporal concentration may greatly increase the received power without increasing the total electromagnetic energy transported within the selected radiation beam, provided that the energy balance is evaluated consistently in a specified observation frame.

The principal objective is therefore to determine whether physically realizable motions of localized electromagnetic sources can produce the arrival-time concentration required for a gamma-ray burst within the proposed source-dependent propagation framework.

The analysis is conditional on the propagation hypothesis introduced in Part C2 and on the assumed properties of the emitting electromagnetic structures. The resulting calculations establish quantitative consequences of these hypotheses, but do not independently demonstrate that electromagnetic propagation in vacuum follows the proposed law or that the mechanism accounts for the observed GRB population.

The following sections introduce the physical source model, derive the arrival-time transformation and its critical condition, examine gravitationally determined source trajectories, calculate representative burst profiles and electromagnetic energy balances, and discuss the observational consequences and limitations of the proposed interpretation. [1], [2], [4], [5]

2. Physical Model of the Gamma-Ray Source

2.1. A Localized Gamma-Emitting Region

The present model investigates gamma-ray bursts (GRBs) as a possible consequence of the temporal concentration of electromagnetic radiation emitted over an extended interval.

The essential physical requirement is not a sudden increase in the intrinsic luminosity of the astronomical source, but the existence of

an emitting region whose motion produces a suitable distribution of electromagnetic propagation velocities and arrival times.

The gamma-ray source is therefore represented as a localized emitting region within a larger astronomical system.

Such a region may be associated with magnetized plasma surrounding a neutron star, a compact object, a binary system, or another environment capable of sustaining high-energy electromagnetic emission.

A neutron star remains a possible component of the source system because of its strong gravitational field, intense magnetic environment, and available energy reservoirs. However, the present model does not require gamma radiation to originate directly from the stellar surface.

This distinction is important because the electromagnetic and dynamical properties of a localized plasma region may differ substantially from those of the underlying compact object.

The emitting region may possess its own velocity, acceleration, electromagnetic field configuration, and characteristic dimensions.

Consequently, the rotational motion of the central astronomical object does not necessarily determine the radial velocities of all gamma-emitting structures.

For temporal concentration, the decisive requirement is that the radiation contributing to a particular observed burst follows sufficiently compatible propagation-time histories.

The model therefore treats the gamma-emitting region as the primary dynamical source, while the surrounding astronomical system determines the physical conditions under which its emission is generated and transported.

2.2. Continuous Energy Supply and Gamma-Ray Emission

A localized emitting region cannot produce electromagnetic radiation indefinitely without receiving energy from its surroundings or consuming an available internal energy reservoir.

The present model therefore distinguishes between the energy source and the region where gamma radiation is generated.

Energy may be supplied through electromagnetic fields, plasma motion, magnetic-field reconfiguration, gravitationally driven flows, or other processes occurring within the astronomical environment.

In particular, electromagnetic energy can enter the emitting region through the Poynting flux associated with the surrounding electric and magnetic fields.

The energy balance of the region may be expressed schematically as

$$P_{\mathrm{in}} - P_{\mathrm{rad}} - P_{\mathrm{other}},$$

where W_{reg} is the energy stored within the emitting region, P_{in} is the supplied power, P_{rad} is the emitted electromagnetic power, and P_{other} represents other energy transfers.

For approximately stationary emission,

$$P_{\mathrm{in}} \approx P_{\mathrm{rad}} + P_{\mathrm{other}}.$$

The intrinsic gamma-ray luminosity may therefore remain approximately constant over a substantial interval, provided that the required energy supply is maintained.

Within the proposed GRB mechanism, the observed burst does not necessarily correspond to a comparable increase in the instantaneous power generated at the source.

Instead, electromagnetic energy emitted over a longer interval may reach the observer within a much shorter period.

The temporal concentration mechanism changes the distribution of received energy in time, but it does not provide an additional energy source.

The physical production of gamma radiation and the transformation of its arrival-time distribution are therefore treated as separate processes.

2.3. Motion and Resultant Acceleration of the Emitting Region

The propagation-time concentration mechanism depends on the radial velocity and acceleration of the emitting region relative to the observer.

The motion of the region may be determined by several physical interactions acting simultaneously.

These may include gravitational forces, electromagnetic forces, pressure gradients, radiation forces, and dynamical interactions with the surrounding plasma.

For an emitting region with effective inertial mass (M), the resultant acceleration may be written as

$$M\mathbf{a}_{\text{net}} = \mathbf{F}_{\text{grav}} + \mathbf{F}_{\text{EM}} + \mathbf{F}_{\text{pressure}} + \mathbf{F}_{\text{other}}$$

The relevant quantity for temporal concentration is the component of this resultant acceleration along the observer's line of sight.

Let u(t) denote the radial velocity of the emitting region toward the observer, with positive values corresponding to approaching motion.

The corresponding radial acceleration is

$$a_r(t) = \frac{du(t)}{dt}.$$

The rate of change of radial acceleration is

$$j_r(t) = \frac{da_r(t)}{dt}.$$

The proposed propagation relation developed in Part C2 assigns an effective propagation speed relative to the observer that depends on the radial velocity of the source.

Consequently, the evolution of u(t), $a_r(t)$, and $j_r(t)$ determines how successive electromagnetic emissions are distributed in observer time.

The required acceleration need not be produced by gravity alone.

In a magnetized plasma, gravitational and electromagnetic contributions may partially reinforce or oppose one another. The resulting radial acceleration can therefore be substantially smaller than the magnitude of individual acceleration components.

This possibility broadens the range of astronomical environments in which the critical propagation condition may occur.

The gravitationally bound binary systems calculated in Sections 4 and 5 remain important quantitative examples. They demonstrate that the required source motion can arise from specified gravitational trajectories without introducing arbitrary acceleration histories.

However, gravitational binary motion is treated as one physically calculable realization of the mechanism, rather than as a universal requirement for all gamma-ray bursts.

2.4. Local Electromagnetic Coherence and Wave Merging

The temporal concentration mechanism requires sufficiently small differences in the propagation histories of electromagnetic structures contributing to the observed burst.

An extended plasma environment may contain many electromagnetic emitting regions with different positions, motions, field configurations, and intrinsic radiation properties.

The present model does not assume that all radiation emitted throughout such an environment propagates with an identical effective velocity.

Instead, a particular observed burst may originate predominantly from a localized region whose electromagnetic structures possess sufficiently compatible propagation characteristics.

Part B2 develops the hypothesis that neighbouring electromagnetic waves or coherent wave chains may undergo structural merging when their spatial field distributions are sufficiently compatible.

The proposed conditions favoring such merging include approximately equal wavelengths, compatible polarization, sufficiently small phase differences, and nearly parallel propagation directions.

During prolonged overlap, the interacting electric and magnetic fields may reorganize into a single coherent electromagnetic structure.

For an idealized merging process without energy losses, the total electromagnetic energy is conserved.

In a common observation frame K,

$$W_1^{(K)} + W_2^{(K)}.$$

Part B2 additionally proposes, as a working hypothesis, that the propagation velocity of the resulting structure may approach the energy-weighted mean of the incoming velocities:

$$\frac{W_1^{(K)} v_1^{(K)} + W_2^{(K)} v_2^{(K)}}{W_1^{(K)} + W_2^{(K)}}.$$

This relationship is a proposed property of electromagnetic structural merging, not a consequence of energy conservation alone.

When the incoming wavelengths are approximately equal and the common wavelength is preserved, the corresponding frequency adjustment is

$$\frac{W_1^{(K)} f_1^{(K)} + W_2^{(K)} f_2^{(K)}}{W_1^{(K)} + W_2^{(K)}}.$$

Such merging could reduce differences among the effective propagation velocities of electromagnetic structures within a localized emitting region.

This possibility is relevant to the GRB model because large differences in propagation velocity would produce substantial differences in arrival time over astronomical distances.

Nevertheless, coherent merging does not automatically guarantee the degree of velocity uniformity required for strong temporal concentration. Its effectiveness depends on the incoming energy distribution, spatial overlap, phase compatibility, and subsequent propagation history.

The present article does not attempt to derive the microscopic dynamics of wave merging or the associated electromagnetic momentum redistribution.

Instead, it treats local coherence and possible structural merging as mechanisms that may help establish sufficiently uniform propagation conditions before radiation begins its long-distance journey toward the observer.

2.5. Spatial Extent and Temporal Synchronization

A physical gamma-emitting region has finite spatial dimensions.

Different parts of the region may occupy different distances from the observer and may possess slightly different radial velocities or accelerations.

Under the source-dependent propagation hypothesis, these differences influence the arrival-time distribution of the emitted radiation.

Let D denote the characteristic source–observer distance and v the effective propagation velocity.

For two electromagnetic structures traveling approximately the same distance, a small propagation-velocity difference Δv produces, to first order, an arrival-time difference of magnitude

$$|\Delta t_p| \approx \frac{D}{v^2} |\Delta v|.$$

For $v \approx c$,

$$|\Delta t_p| \approx \frac{D}{c^2} |\Delta v|.$$

Thus, even extremely small differences in effective propagation velocity can produce

significant arrival-time differences over cosmological distances.

For example, at a distance of 2.1 billion light-years, an arrival-time difference of three seconds corresponds approximately to

$$|\Delta v| \approx 1.36 \times 10^{-8}\ \mathrm{m/s}.$$

This estimate illustrates the exceptional sensitivity of the proposed temporal-concentration mechanism to variations in propagation velocity.

It does not imply that every electromagnetic structure throughout a large plasma environment must satisfy this condition.

The requirement applies to the subset of radiation intended to contribute to the same narrow observational interval, after accounting for its emission times and positions.

The spatial dimensions of the emitting region introduce an additional geometrical contribution.

For a characteristic line-of-sight depth $L_{\parallel}$, the purely geometrical arrival-time spread is approximately

$$\Delta t_{\mathrm{geom}} \approx \frac{L_{\parallel}}{c},$$

when propagation velocities are close to c.

The complete arrival-time distribution must therefore account for emission time, position, effective propagation velocity, and their possible correlations.

A spatially extensive astronomical environment may contain several localized emitting regions that independently satisfy, or fail to satisfy, the temporal-concentration condition.

Radiation from regions with sufficiently compatible arrival-time histories may contribute to the same gamma-ray maximum.

Radiation from other regions may arrive over substantially longer intervals and form weaker or broader components.

The relevant synchronization is therefore a property of the participating radiation and its propagation history, rather than a requirement for uniform motion of the entire astronomical source.

2.6. Gamma-Ray Energy and Source Diversity

The proposed model allows a wide range of gamma-ray source environments, emission powers, and durations.

For approximately constant gamma-ray luminosity L_{γ} over an emission interval T_e, the emitted energy is

$$W_{\gamma} = L_{\gamma} T_e.$$

If the radiation contributing to the observed burst is concentrated into a shorter interval T_p, the mean temporal concentration factor is

$$\overline{K} = \frac{T_e}{T_p}.$$

Under the idealized assumption that the energy transported within a selected radiation beam is conserved, the mean received power is increased by this concentration factor relative to the same beam without temporal compression.

The concentration factor does not determine the total emitted energy.

A relatively weak source emitting over a long interval may produce a pronounced observational maximum, while a more energetic source may produce a much greater integrated burst energy.

The absolute intensity observed on Earth additionally depends on emission directionality, propagation distance, beam geometry, and possible energy losses.

The model therefore does not require all gamma-ray bursts to originate from identical objects or to share a universal luminosity.

Different astronomical environments may possess different energy reservoirs and electromagnetic transport mechanisms.

Likewise, different emitting regions may have distinct velocity histories, radial accelerations, acceleration gradients, and spatial dimensions.

These differences can produce substantial variations in the duration, intensity, and temporal structure of the observed gamma-ray emission.

The proposed temporal-concentration mechanism does not eliminate the requirement for a physically adequate source of gamma-ray energy.

Rather, it separates the energy needed to produce the radiation from the propagation conditions that determine how rapidly that energy reaches the observer.

2.7. Scope and Principal Assumptions of the Source Model

The present model separates three physical processes:

1. The supply and conversion of energy into gamma radiation within an astronomical environment.
2. The establishment of sufficiently compatible electromagnetic propagation characteristics within a localized emitting region.
3. The temporal redistribution of radiation arrival times resulting from the motion and acceleration of the emitting region.

The first process concerns the astrophysical production of electromagnetic energy.

The second concerns the possible organization and structural merging of electromagnetic waves, investigated separately in Part B2.

The third is described by the source-dependent propagation relation proposed in Part C2 and quantitatively developed in the following sections of this article.

The principal working assumptions are:

- Gamma radiation may originate from localized regions of magnetized plasma or other compact electromagnetic environments, without requiring direct emission from the surface of a non-rotating neutron star.
- The emitting region has a physically determined radial velocity and resultant acceleration.
- Gravitational motion is one possible cause of the required acceleration, while electromagnetic and other forces may also contribute.
- A subset of electromagnetic radiation may possess sufficiently compatible propagation histories to produce strong temporal concentration.
- Coherent electromagnetic merging may contribute to local propagation-velocity adjustment, but its quantitative effectiveness remains a hypothesis.
- The energy carried by the selected radiation beam is conserved under idealized loss-free propagation, with the energy balance evaluated in a specified observation frame.
- Radiation from different emitting regions may produce distinct temporal and spectral components.

The model does not assume that all astronomical gamma radiation originates from the same physical mechanism.

Nor does it require the entire astronomical environment to exhibit uniform motion or identical electromagnetic properties.

Its central hypothesis is that a physically localized source of sustained electromagnetic radiation can, under suitable radial acceleration and propagation conditions, produce an intense observational event through the temporal concentration of previously emitted energy.

The following sections derive the corresponding arrival-time transformation, determine its critical condition, and examine quantitatively whether gravitationally

determined source trajectories can produce the required temporal concentration.

These calculations are conditional on the proposed source-dependent propagation law. They do not independently establish that electromagnetic propagation in vacuum follows this law, nor do they demonstrate that the proposed mechanism accounts for the observed gamma-ray burst population. [6], [7], [8]

3. Propagation and Temporal Concentration

3.1. Source-Dependent Propagation

The proposed model considers electromagnetic radiation emitted from a localized region within a larger astronomical environment. The emitting region may be associated with magnetized plasma, a compact astronomical object, or another system capable of sustained gamma-ray emission.

The propagation model adopts the source-dependent velocity hypothesis developed in Part C2. According to this hypothesis, the propagation velocity of electromagnetic radiation relative to the observer depends on the radial velocity of the emitting source at the time of emission.

Let K denote the observation frame in which the receiving observer is at rest. Let t_e be the emission time and $u(t_e)$ the radial velocity of the emitting region toward the observer, with positive values corresponding to approaching motion.

For an electromagnetic structure leaving the emitting region, the proposed propagation velocity is

$$v(t_e) = c + u(t_e).$$

The emitted radiation may have undergone local electromagnetic interactions before leaving the source region. Part B2 considers the possibility that compatible electromagnetic waves or coherent chains merge into common structures, with their propagation characteristics adjusted during the merging process.

Such local reorganization may contribute to reducing the differences between the propagation velocities of electromagnetic structures emerging from the same region.

In the present calculation, the effective velocity of the outgoing radiation is assumed to follow the radial motion of the emitting region sufficiently closely that the source-dependent propagation relation remains applicable.

After leaving the local formation region, each electromagnetic structure is assigned the propagation velocity corresponding to its emission time. Further changes of this velocity during long-distance propagation are neglected in the primary calculation.

Let $D(t_e)$ denote the distance between the emitting region and the observer at the emission time. The corresponding arrival time is

$$t_p = t_e + \frac{D(t_e)}{c + u(t_e)}.$$

The source distance changes as the emitting region moves. With the adopted sign convention,

$$\frac{dD}{dt_e} = -u(t_e).$$

These relations provide the basis for calculating the arrival-time distribution of radiation emitted during an extended interval.

When the radial velocity of the emitting region changes, successive

electromagnetic structures are assigned different propagation velocities. Consequently, the intervals between their arrivals need not be equal to the intervals between their emissions.

Under suitable acceleration conditions, radiation emitted over a long interval may reach the observer within a much shorter interval, producing temporal concentration.

The present formulation distinguishes local electromagnetic structure formation from subsequent long-distance propagation. The detailed field dynamics of wave merging is not included in the arrival-time calculation.

The relation v=c+u remains an explicit hypothesis of Part C2 rather than a result derived from standard vacuum Maxwell theory. The following sections investigate its mathematical consequences for the arrival times and temporal concentration of gamma radiation.

3.2. Arrival-Time Gradient

The source distance changes with its radial motion. With the chosen sign convention,

$$\frac{dD}{dt_e} = -u, \qquad a = \frac{du}{dt_e}$$

Differentiating the arrival-time relation gives

$$\frac{dt_p}{dt_e} = \frac{c}{c+u} - \frac{Da}{(c+u)^2}$$

Define the arrival-time gradient J:

$$J(t_e) = \frac{dt_p}{dt_e} = \frac{c(c+u) - Da}{(c+u)^2}$$

When $|J|$ is small, an extended emission interval is mapped into a much shorter interval of arrival times. Both positive and negative branches of J may contribute radiation at a common observation time if the mapping is not one-to-one.

3.3. Critical Condition for Temporal Concentration

A stationary point of the arrival-time mapping occurs when $J = 0$. The exact critical condition is

$$D(t_e)a(t_e) = c[c + u(t_e)]$$

For $|u| \ll c$, the approximate critical radial acceleration becomes

$$a_{\text{crit}} \approx \frac{c^2}{D}$$

The critical value is inversely proportional to source distance and concerns the component of acceleration directed toward the observer, not necessarily the total gravitational acceleration. Natural gravitational motions can satisfy this condition at particular positions and times.

A stationary point alone does not specify a gamma-ray burst. The duration and intensity also depend on how quickly the arrival-time gradient changes, on the emission interval, and on the dimensions and dynamics of the emitting region.

3.4. Local Expansion Around a Critical Point

Let t_0 be an emission time satisfying the critical condition and write $\tau = t_e - t_0$. Near the critical time the radial acceleration can be expanded as

$$a(t_e) \approx a_0 + j_0\tau$$

where $j_0 = da/dt_e$ at t_0 is the radial jerk. Differentiation of the exact expression for J, evaluated at $J(t_0) = 0$, yields

$$J'(t_0) = \frac{(c+u_0)a_0 - D_0 j_0}{(c+u_0)^2}$$

To second order in emission-time offset,

$$t_p(t_0+\tau)-t_p(t_0)\approx\frac{1}{2}J'(t_0)\tau^2$$

For $|u_0|\ll c$ and when the term involving j_0 dominates the smaller contribution a_0/c, this becomes

$$|\Delta t_p|\approx\frac{D_0|j_0|}{2c^2}\tau^2\approx\frac{|j_0|}{2a_{\text{crit}}}\tau^2$$

For an emission interval T_e beginning at the critical point, its approximate arrival-time span is

$$T_p\approx\frac{D_0|j_0|T_e^2}{2c^2}$$

Therefore, the required local jerk for a chosen emission and observed interval is

$$|j_0|\approx\frac{2c^2T_p}{D_0T_e^2}$$

These expressions are **local approximations**. For days, months, or longer emission intervals the full trajectories $D(t_e)$ and $u(t_e)$ must be inserted into the exact arrival-time equation. A small jerk at one instant does not guarantee sustained concentration.

3.5. Multiple Emission Times and Temporal Caustics

The arrival-time mapping need not be one-to-one. Near a local maximum or minimum, several emission times may correspond to the same observed time. The resulting *temporal caustic* can have an exceptionally high received flux because distinct emission intervals contribute together.

For incoherently additive radiation contributions in a specified ray bundle, the received power is formally

$$P_p(t_p)=\sum_i\frac{P_e(t_{e,i})}{|J(t_{e,i})|}$$

The sum includes all emission times $t_{e,i}$ corresponding to the same t_p. The ideal point-source formula can become singular at the stationary point, although the integral across the caustic is finite. Finite emitting regions, finite temporal resolution, and overlapping electromagnetic fields constrain the measurable peak.

If wave chains overlap coherently, their electromagnetic fields must be combined before the Poynting flux is evaluated. The model of coherent-wave structural evolution is developed in Part B2 and is not rederived here.

3.6. Energy Redistribution and Observational Consequences

Temporal concentration redistributes electromagnetic energy in observer time; it does not create energy. Provided the transmitted energy in the considered radiation bundle is conserved,

$$\int P_p(t_p)\,dt_p=\int P_e(t_e)\,dt_e$$

For approximately steady emission over T_e, concentrated into an arrival interval T_p, the mean temporal concentration factor is

$$K=\frac{T_e}{T_p}$$

Consequently, a short high-intensity gamma-ray maximum may be associated with a much longer emission history. Variations in source distance, radial gravitational motion, jerk, emission duration, and observation geometry generate different burst durations and temporal profiles. Gravitationally calculated examples are developed in the following sections.

The analysis is conditional on the propagation relation adopted from Part C2. It derives the arrival-time consequences of that premise rather than

independently verifying the propagation law.

4. Gravitational Motion of the Source

4.1. Natural Origin of the Radial Acceleration

The temporal concentration mechanism developed in Section 3 requires a particular evolution of the radial velocity of the gamma-ray source. This evolution need not be prescribed as an arbitrary function. It may follow from the gravitational motion of a compact object in a bound astronomical system.

The central quantity is not the total gravitational acceleration, but its component along the line of sight to the observer. Even if the magnitude of the gravitational acceleration changes little, its radial projection may vary as the source moves along a curved trajectory. A passage through the critical condition therefore depends jointly on the gravitational field and the viewing geometry.

Let M_1 be the mass of the gamma-emitting neutron star, M_2 the mass of its companion, and r their instantaneous separation. In the Newtonian approximation, the acceleration of the neutron star relative to an inertial frame is directed toward the companion and has magnitude

$$a_g = \frac{GM_2}{r^2}$$

The line-of-sight component is

$$a_{\parallel} = a_g \cos\alpha$$

where α is the angle between the acceleration vector and the direction toward the observer. The sign convention throughout the article is that positive u denotes motion toward the observer.

The critical condition derived in Section 3 is

$$D(t_e)a_{\parallel}(t_e) = c[c + u(t_e)]$$

For $|u| \ll c$, the required radial acceleration is approximately

$$a_{\mathrm{crit}} \simeq \frac{c^2}{D}$$

Consequently, a gravitational system can cross the critical condition whenever its accessible line-of-sight acceleration includes this value. This is a necessary kinematic condition, not in itself a prediction of a detectable burst.

4.2. A Gravitationally Bound Binary System

A neutron star and a companion star provide a useful example because their motion can be calculated from their masses and orbital geometry. A circular orbit is adopted first to isolate the temporal-concentration mechanism without introducing additional orbital parameters. The approach can subsequently be extended to eccentric orbits.

For a binary with constant separation r, the angular frequency of its relative motion is

$$\Omega = \sqrt{\frac{G(M_1 + M_2)}{r^3}}$$

The distance of the neutron star from the system barycentre is

$$r_1 = \frac{M_2}{M_1 + M_2} r$$

Its orbital speed and acceleration are

$$v_1 = r_1 \Omega$$

$$a_1 = r_1\Omega^2 = \frac{GM_2}{r^2}$$

The orbital period is

$$P_{\mathrm{orb}} = \frac{2\pi}{\Omega}$$

These relations show that the radial velocity history is constrained by a definite gravitational trajectory. The acceleration and its rate of change cannot be adjusted independently once the masses, orbital separation, and viewing geometry have been specified.

4.3. Line-of-Sight Geometry and the Critical Crossing

Consider first an edge-on circular orbit, with its orbital plane containing the line of sight. Let $x(t_e)$ denote the source displacement toward the observer relative to the binary barycentre, and define

$$\theta(t_e) = \theta_0 + \Omega t_e$$

$$x(t_e) = r_1\cos\theta(t_e)$$

The corresponding radial velocity, acceleration, and rate of change of acceleration are

$$u(t_e) = -r_1\Omega\sin\theta(t_e)$$

$$a_{\parallel}(t_e) = -r_1\Omega^2\cos\theta(t_e)$$

$$j_{\parallel}(t_e) = r_1\Omega^3\sin\theta(t_e)$$

The source–observer distance is, to the accuracy of the far-field binary approximation,

$$D(t_e) = D_0 - x(t_e)$$

At a critical emission time t_0, the exact arrival-time condition becomes

$$[D_0 - r_1\cos\theta_0](-r_1\Omega^2\cos\theta_0) = c[c - r_1\Omega\sin\theta_0]$$

This equation determines a possible critical orbital phase; it is not an independently imposed acceleration profile. In the distant-source, low-speed limit, the condition reduces to

$$-a_1\cos\theta_0 \simeq \frac{c^2}{D_0}$$

A critical phase can therefore exist only if

$$a_1 \geq a_{\mathrm{crit}}$$

For an inclination i defined such that $i = 90^\circ$ corresponds to an edge-on orbit, the maximum radial acceleration is $a_1\sin i$. The more general necessary condition is

$$a_1\sin i \geq a_{\mathrm{crit}}$$

In the simplified low-speed approximation, this provides an upper bound on the orbital separation for a given companion mass and inclination:

$$r \lesssim \sqrt{\frac{GM_2D_0\sin i}{c^2}}$$

A sufficiently distant binary orbit may thus have too little projected acceleration to reach a true stationary point of the arrival-time map. This constraint must be checked together with the required temporal width.

4.4. Natural Variation of Radial Acceleration

The temporal width of a concentration event depends on how rapidly the arrival-time gradient changes around its stationary point. For a circular binary, the largest possible magnitude of the radial acceleration derivative is

$$j_{\max} = a_1\Omega$$

or, equivalently,

$$j_{\max} = \frac{GM_2}{r^2}\sqrt{\frac{G(M_1 + M_2)}{r^3}}$$

Thus, for fixed stellar masses,

$$j_{\max} \propto r^{-7/2}$$

Increasing the binary separation generally reduces the acceleration derivative. However, it also reduces the available gravitational acceleration as r^{-2}. A small value of j alone is therefore insufficient: the orbit must still reach the critical line-of-sight acceleration.

For comparison, the radial component of the acceleration of a body falling toward a stationary mass changes according to

$$a_g = \frac{GM}{r^2}$$

$$\left|\frac{da_g}{dt_e}\right| = \frac{2GM|\dot{r}|}{r^3}$$

Radial infall and curved orbital motion are consequently two distinct routes to a varying line-of-sight acceleration. Neither needs to be excluded a priori; their viability is determined by the complete arrival-time mapping and the physical properties of the emitting object.

4.5. Temporal Width Near a Critical Orbital Phase

Let the arrival-time gradient be

$$J(t_e) = \frac{dt_p}{dt_e}$$

At a stationary point t_0, $J(t_0) = 0$. The first non-vanishing term of the local arrival-time expansion is ordinarily quadratic:

$$t_p(t_e) - t_p(t_0) \simeq \frac{1}{2}J'(t_0)(t_e - t_0)^2$$

For the source-dependent propagation rule adopted in this article, and using the exact critical condition, its curvature is

$$J'(t_0) = \frac{(c + u_0)a_0 - D_0 j_0}{(c + u_0)^2}$$

Here D_0, u_0, a_0, and j_0 refer to the values at the critical emission time. This expression makes explicit that the temporal curvature depends on both the acceleration and its derivative. Where the term $D_0 j_0$ dominates and $|u_0| \ll c$, it reduces to

$$J'(t_0) \simeq -\frac{D_0 j_0}{c^2}$$

For emission extending from the critical instant over a duration T_e, a useful local estimate of the arrival-time span is

$$T_p \simeq \frac{|J'(t_0)|}{2} T_e^2$$

and, under the additional approximation above,

$$T_p \simeq \frac{D_0|j_0|}{2c^2} T_e^2$$

These relations are local approximations. Their accuracy for hours, days, or months of emission must be verified against the complete orbital map, especially when higher derivatives become relevant or when the map has multiple branches.

4.6. Limits and Role in the Quantitative Examples

The gravitational calculation establishes that a stationary point of the arrival-time transformation can arise from natural source motion, provided the projected acceleration reaches the critical value. It also identifies the competing roles of orbital separation: more distant orbits may sustain a slowly varying acceleration, but eventually fail to reach the critical threshold.

The calculation does not determine gamma-ray production, the radiative efficiency of a localized plasma region, or the observability of the resulting signal. These remain distinct physical questions. The gravitational examples assume that a localized emitting region approximately shares the calculated orbital motion,

without requiring direct emission from a stellar surface or negligible neutron-star rotation.

Section 5 evaluates specific binary configurations using the full time-dependent distance and radial velocity, compares their calculated arrival-time spans, and distinguishes temporal concentration from the separate requirements of gamma-ray luminosity and integrated energy. [1], [2]

5. Quantitative Examples

5.1. Purpose and Common Parameters

Sections 3 and 4 establish the arrival-time transformation proposed in Part C2 and show how a sufficiently small arrival-time gradient may arise from the radial motion of an emitting region. This section evaluates three circular binary configurations in which continuous electromagnetic emission over different intervals is mapped into substantially shorter intervals at a distant observer. These calculations are conditional examples of the proposed propagation law; they are not fits to identified gamma-ray bursts.

The physical emitter is taken to be a localized gamma-emitting region within the environment of a neutron star. For the three numerical examples, this region is assumed to move approximately together with the neutron star's orbital motion. The radiation is **not** required to originate at the stellar surface, and the calculations do not require the neutron star to be non-rotating. Motions of the plasma relative to the star, electromagnetic accelerations, and structural adjustments of outgoing electromagnetic waves are excluded from these particular orbital examples. They remain possible effects in the more general source model of Section 2.

All three calculations use the same hypothetical binary, consisting of a neutron star with mass $M_1 = 1.4M_\odot$ and a companion with mass $M_2 = 1.0M_\odot$. The adopted source–observer distance is $D_0 = 2.1 \times 10^9$ ly. The binary separation r and the initial orbital phase θ_0 differ among the examples. The receiving observer defines the common observation frame for the radial velocities and arrival times.

For a circular binary, the orbital angular frequency and the neutron star's barycentric orbital radius are

$$\Omega = \sqrt{\frac{G(M_1 + M_2)}{r^3}},$$

$$r_1 = \frac{M_2}{M_1 + M_2}\, r.$$

For the edge-on geometry used in the calculations, the radial source velocity toward the observer and the source–observer distance are expressed as

$$u(t_e) = -r_1 \Omega \sin(\theta_0 + \Omega t_e),$$

$$D(t_e) = D_0 - r_1 \cos(\theta_0 + \Omega t_e).$$

The sign convention assigns positive u to motion toward the observer, so that $dD/dt_e = -u$. With the source-dependent propagation relation used throughout the orbital calculation, the modeled arrival time is

$$t_p(t_e) = t_e + \frac{D(t_e)}{c + u(t_e)}.$$

This expression assumes that outgoing electromagnetic structures have an effective speed $c + u(t_e)$ in the observer's frame and that any subsequent changes in that speed are negligible for the modeled flight. Possible local wave merging,

discussed in Part B2, is assumed not to introduce an additional time-dependent velocity offset in these examples.

Only arrival-time differences are evaluated, because the absolute propagation time is of the order of billions of years. For each orbit, the starting phase is selected by the stationary-arrival condition

$$D(0)a(0) = c\,[c + u(0)],$$

where $a(t_e) = du/dt_e$ is the line-of-sight acceleration. Once this phase is determined, the arrival-time difference over the chosen emission interval is evaluated using the complete orbital expression rather than an arbitrarily imposed acceleration history.

The calculations neglect finite emitting-region size, velocity dispersion within the plasma, cosmological propagation corrections, and losses. Their purpose is to isolate the temporal-concentration effect generated by gravitationally determined motion. Section 5.6 states how these idealizations limit the astrophysical interpretation.

5.2. One Hour of Emission: A 44 AU Binary

For a binary separation of $r = 44\,\mathrm{AU}$, Newtonian two-body dynamics gives an orbital period of approximately 188.4 years and a neutron-star orbital speed of approximately $2.90\,\mathrm{km\,s^{-1}}$. The gravitational acceleration due to the companion is $3.06 \times 10^{-6}\,\mathrm{m\,s^{-2}}$, considerably above the critical line-of-sight acceleration at the adopted distance.

The appropriate orbital orientation gives a critical instant at which the projected acceleration satisfies the condition derived in Section 3. Its local rate of change is approximately

$$j_0 = -3.237 \times 10^{-15}\,\mathrm{m\,s^{-3}}$$

A one-hour emission interval beginning at that instant produces the following arrival-time interval under the full orbital mapping:

$$T_e = 3600\,\mathrm{s} \quad \rightarrow \quad T_p = 4.637\,\mathrm{s}$$

The mean temporal concentration factor is

$$K = \frac{T_e}{T_p} \approx 776$$

This is the short-emission example. It demonstrates that the radial acceleration required by the model can be produced by a familiar gravitational equation, with the small observed acceleration arising from its line-of-sight projection rather than from an artificially weak gravitational force.

5.3. One Day of Emission: A 306.3 AU Binary

Increasing the binary separation decreases the gravitational acceleration and the rate at which its projection changes. For $r = 306.3\,\mathrm{AU}$, the orbital period is approximately 3460 years, the neutron star's orbital speed is approximately $1.10\,\mathrm{km\,s^{-1}}$, and its gravitational acceleration is approximately $6.32 \times 10^{-8}\,\mathrm{m\,s^{-2}}$.

At the critical orbital phase, the local acceleration gradient has the value

$$j_0 = -3.628 \times 10^{-18}\,\mathrm{m\,s^{-3}}$$

The exact arrival-time difference for a continuous 24-hour emission interval is

$$T_e = 86400\,\mathrm{s} \quad \rightarrow \quad T_p = 2.993\,\mathrm{s}$$

Accordingly,

$$K = \frac{86400}{2.993} \approx 2.89 \times 10^4$$

The result is not obtained by keeping the motion of the 44 AU system and simply

extending its emission time. It follows from a different gravitational orbit, whose smaller orbital frequency gives a much slower evolution of the projected acceleration near the critical phase.

5.4. Thirty Days of Emission: A 1141.414 AU Binary

A more demanding test is whether the proposed propagation law can concentrate an entire month of emission into a few seconds. For the same masses and distance, a circular binary separation of approximately $1141.414\,\mathrm{AU}$ yields an orbital period of approximately $24{,}892$ years and a neutron-star orbital speed of approximately $63\,\mathrm{m\,s^{-1}}$ **in the observer direction at the selected critical phase**; its full orbital speed is approximately $569\,\mathrm{m\,s^{-1}}$.

The gravitational acceleration is approximately $4.55 \times 10^{-9}\,\mathrm{m\,s^{-2}}$. This is only slightly greater than the required critical acceleration, $a_{\mathrm{crit}} \simeq 4.524 \times 10^{-9}\,\mathrm{m\,s^{-2}}$. Consequently, the critical phase occurs close to maximum acceleration toward the observer. The rate of change of the radial acceleration is

$$j_0 = -4.040 \times 10^{-21}\,\mathrm{m\,s^{-3}}$$

Evaluating the full arrival-time mapping over 30 days gives

$$T_e = 2\,592\,000\,\mathrm{s} \quad \rightarrow \quad T_p = 3.000\,\mathrm{s}$$

The corresponding mean temporal concentration factor is

$$K = \frac{2\,592\,000}{3.000} = 864\,000$$

This month-long example is particularly informative because the critical condition and the required small j are both satisfied by the same orbit. A small j alone would not be sufficient if the total gravitational acceleration fell below the critical value. At the adopted masses and distance, the limiting binary separation at which the available gravitational acceleration equals the critical acceleration is approximately $1145\,\mathrm{AU}$. The 30-day configuration lies close to that boundary.

5.5. Comparison of the Three Calculations

Emission interval	Separation (AU)	Orbital period (yr)	Projected jerk at critical phase (m s⁻³)	Arrival interval (s)	Mean concentration
1 hour	44.0	188.4	−3.237 × 10⁻¹⁵	4.637	776
1 day	306.3	3,460	−3.628 × 10⁻¹⁸	2.993	28,866
30 days	1,141.414	24,892	−4.040 × 10⁻²¹	3.000	864,000

Table 1*. Three idealized binary systems calculated with identical component masses and observer distance. Orbital acceleration and its time derivative follow from two-body gravitation; the source-dependent arrival-time law is a separate model assumption. The listed emission intervals begin at a critical instant and continue on one side of it.*

Near a nondegenerate critical point, the local arrival-time relation may be approximated by

$$t_p - t_{p,0} \simeq \frac{J'(t_0)}{2}(t_e - t_0)^2$$

where $J = dt_p/dt_e$. In the regime where the term involving Dj dominates the local curvature, the resulting time interval is approximately

$$T_p \simeq \frac{D_0|j_0|}{2c^2} T_e^2$$

Thus, at fixed D_0 and target T_p, a longer concentrated emission interval requires a smaller magnitude of the local acceleration gradient:

$$|j_0| \propto T_e^{-2}$$

The local estimate is a guide, not a replacement for orbital integration. The full model must also satisfy the critical acceleration condition and account for the higher derivatives of the source motion over the entire emission interval. In the examples above, direct evaluation of the orbital arrival-time relation provides the reported intervals.

5.6. Interpretation, Energy and Limitations

The three examples demonstrate that distinct circular binary configurations can generate substantially different ratios of emission duration to arrival duration within the source-dependent propagation model. With the same component masses and observer distance, the computed configurations map emission lasting one hour, one day, and thirty days into intervals of approximately 4.637 s, 2.993 s, and 3.000 s, respectively. The corresponding mean concentration factors are approximately 776, 28,866, and 864,000. These values follow from the specified orbital trajectories and the assumed arrival-time relation; they do not establish that observed GRBs are generated by this mechanism.

The neutron star in these examples supplies a gravitationally calculable orbital trajectory for the localized emitting region. It need not be the radiating surface itself. A magnetized plasma region may receive energy from a larger electromagnetic environment and emit radiation while approximately sharing the star's barycentric motion. The calculations do not independently establish that such an emitting region can sustain the required gamma-ray luminosity or maintain the required uniformity of effective propagation velocities.

Let $L_e^{(K)}$ be the power assigned to a selected outgoing radiation beam during an emission interval T_e, with energy and power consistently defined in the same observation frame K. For approximately steady emission, its energy is

$$W_e^{(K)} = L_e^{(K)} T_e.$$

If that beam experiences ideal temporal redistribution without energy loss or exchange with other degrees of freedom, its energy within the same frame is conserved. The mean equivalent power over the compressed arrival interval T_p is then

$$\overline{L}_p^{(K)} = \frac{W_e^{(K)}}{T_p} = L_e^{(K)} \frac{T_e}{T_p}.$$

Thus, the mean temporal-concentration factor $\overline{K} = T_e/T_p$ increases the power associated with the selected beam without increasing its integrated energy. This is a time-mapping result, not an independent prediction of the absolute power intercepted by a terrestrial detector. Beaming geometry, geometric dilution, attenuation, and cosmological effects must be considered when converting the beam energy into an observable fluence.

The assumption of energy conservation must also be expressed within a specified observation frame. If an alternative model assigns different electromagnetic energies to the same propagating structure in the source and observer frames, the corresponding energy transformation must be stated before those energies can

be compared. The present examples do not derive that transformation.

The strongest physical limitation concerns the uniformity of arrival-time histories. The selected radiation must originate from positions, times, and motions whose resulting propagation histories remain compatible over an enormous distance. Small differences in radial velocity or effective outgoing-wave speed may broaden or suppress the temporal concentration. Spatial extent, local plasma motions, electromagnetic acceleration, and continuing interactions or wave merging along the path therefore require quantitative assessment. In particular, the energy-weighted velocity-adjustment rule proposed in Part B2 is a working hypothesis and does not by itself demonstrate sufficiently small velocity dispersion.

The orbit-only examples also omit the potentially important contribution of electromagnetic, pressure, and other forces to the *resultant* acceleration of a plasma emitting region. Such forces could either assist or oppose the gravitational acceleration. They broaden the possible physical realizations of the model, but cannot be introduced into the three numerical examples without recalculating the complete source trajectory and arrival-time mapping.

Finally, a high temporal-concentration factor does not resolve the separate energy-budget problem. A detectable GRB still requires a source capable of supplying the integrated gamma-ray energy within the relevant beam, while the production of its spectrum and any broader afterglow remain independent physical constraints.

The quantitative conclusion of this section is therefore specific but conditional: **within the assumed propagation relation**, Newtonian binary motion can produce strong temporal concentration for an idealized localized gamma-emitting region sharing the modeled orbital motion. It is not necessary to assume direct surface emission or negligible stellar rotation. Section 6 examines the corresponding idealized temporal profiles, multiple arrival-time branches, and finite-source effects.

6. Temporal Profiles of Gamma-Ray Bursts

6.1. From Emission Time to the Observed Light Curve

The calculations in Section 5 establish how extended emission intervals may be concentrated into short arrival-time intervals within the proposed source-dependent propagation model. The present section determines the shape of the resulting light curve. The essential distinction is between the duration of a burst and the temporal distribution of its received energy.

Let t_e denote emission time, t_p arrival time, and $g(t_e)$ the arrival-time mapping obtained from the source trajectory. The local Jacobian J is

$$t_{\mathrm{p}} = g(t_{\mathrm{e}}), \quad J(t_{\mathrm{e}}) = \frac{dt_{\mathrm{p}}}{dt_{\mathrm{e}}}$$

The emitting region is initially represented by a point source with a steady luminosity L_e in the radiation beam being followed. If the same electromagnetic energy is conserved during propagation, the received power in a single monotonic branch is the source power divided by the absolute arrival-time gradient:

$$L_{\mathrm{p}}(t_{\mathrm{p}}) = \frac{L_{\mathrm{e}}(t_{\mathrm{e}})}{|J(t_{\mathrm{e}})|}$$

If different emission instants map to the same arrival time, all contributing

branches must be included. Here each branch is treated as an independently averaged energy contribution; phase-coherent interference would require calculation from the combined electromagnetic fields.

$$L_{\mathrm{p}}(t_{\mathrm{p}}) = \Sigma_{\mathrm{i}} \frac{L_{\mathrm{e}}(t_{\mathrm{e,i}})}{|J(t_{\mathrm{e,i}})|}$$

These expressions refer to the conserved energy carried by a selected radiation beam. The measured flux on Earth additionally depends on beam geometry, distance, detector area, and possible propagation losses.

6.2. The Local Shape Near a Critical Arrival Time

At a critical emission time t_o, the arrival-time gradient vanishes. Expanding the complete mapping in the immediate neighbourhood of that point gives

$$J(t_0) = 0$$

$$t_{\mathrm{p}} - t_{\mathrm{p},0} \approx A(t_{\mathrm{e}} - t_0)^2$$

$$A = \frac{J'(t_0)}{2}$$

The coefficient A is determined by the trajectory, not freely imposed on the observed pulse. For the arrival-time law employed in Sections 3–5, its exact local value is

$$J'(t_0) = \frac{(c + u_0)a_0 - D_0 j_0}{(c + u_0)^2}$$

where a_o is the line-of-sight acceleration and j_o its time derivative at the critical instant. When the second term dominates, the local pulse width is primarily controlled by the gradient of acceleration. The full expression must be used when these terms are comparable.

For one emission branch extending from the critical instant, the mapping is quadratic and the idealized received power follows a square-root singularity:

$$L_{\mathrm{p}}(\tau) = \frac{L_{\mathrm{e}}}{2\sqrt{(|A|\tau)}}, \quad 0 < \tau \leq T_{\mathrm{p}}$$

$$\tau = |t_{\mathrm{p}} - t_{\mathrm{p},0}|, \quad T_{\mathrm{p}} = |A|{T_{\mathrm{e}}}^2$$

The divergence at τ = 0 is integrable. It describes an ideal point-source caustic and must not be interpreted as an infinite measurable luminosity.

6.3. A Thirty-Day Emission Interval Concentrated into Three Seconds

For the 30-day example of Section 5, the interval between the critical emission instant and the end of the modelled emission is T_e = 2,592,000 s, while the arrival interval is T_p = 3 s. The corresponding quadratic coefficient and mean concentration factor are

$$A = \frac{3}{(2{,}592{,}000)^2}\, s^{-1} \approx 4.465 \times 10^{-13}\, s^{-1}$$

$$K = \frac{T_{\mathrm{e}}}{T_{\mathrm{p}}} = 864{,}000$$

For a steady source, the accumulated fraction of the emitted energy received by time τ is

$$F(\tau) = \frac{E_{\mathrm{p}}(0,\tau)}{E_{\mathrm{p}}(0,T_{\mathrm{p}})} = \sqrt{(\frac{\tau}{T_{\mathrm{p}}})}$$

Arrival time τ	Accumulated energy	Energy remaining
0.03 s	10.0%	90.0%
0.30 s	31.6%	68.4%
1.00 s	57.7%	42.3%
2.00 s	81.6%	18.4%
3.00 s	100%	0%

***Table 2**. Cumulative energy within the idealized three-second arrival interval. The early arrival phase contains a*

disproportionately large fraction of the total energy.

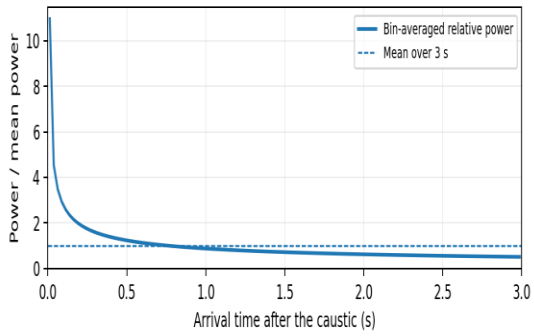


Figure 1. *Idealized one-sided temporal-caustic profile for a 30-day emission interval mapped into three seconds. Values show power averaged in 0.025 s bins; the finite height depends on the bin width and is not an intrinsic maximum.*

The conventional T_{90} interval, defined between 5% and 95% of the accumulated received energy, differs from the full model interval. For this ideal curve it is

$$T_{90} = (0.95^2 - 0.05^2)T_{\mathrm{p}} = 0.90T_{\mathrm{p}} = 2.70\ s$$

Consequently, care is needed when comparing a theoretical arrival window directly with catalogue GRB durations, which commonly use T_{90}.

6.4. More Than One Emission Branch and Multiple Peaks

The arrival-time transformation need not be monotonic. Depending on the gravitational motion of the emitting source, different emission times may correspond to the same observation time.

A single stationary point of the arrival-time mapping can connect two emission branches. Radiation originating from these branches may contribute to the same observed intensity maximum. The contributions increase the received energy flux, provided the corresponding emission intervals overlap in arrival time.

More complex temporal profiles become possible when the arrival-time gradient crosses zero at two or more distinct emission times:

$$J(t_1) = J(t_2) = 0, \qquad t_1 \neq t_2.$$

Each stationary point may generate a temporal caustic. The separation of the corresponding observed maxima is determined by

$$\Delta t_p = |g(t_2) - g(t_1)|.$$

The existence of two critical points does not, by itself, guarantee two closely spaced observed peaks.

For a neutron star in a circular binary orbit, the line-of-sight acceleration varies periodically. If its maximum value exceeds the critical acceleration required by the source-dependent propagation model, the arrival-time gradient may cross zero twice during the corresponding orbital phase interval.

The two crossings can produce separate temporal concentrations of radiation, provided that the source emits during both contributing intervals. Their observed separation and relative intensities depend on the complete orbital trajectory, the intrinsic emission history, and the finite spatial extent of the emitting region.

Consequently, multiple peaks may arise without requiring separate explosive events at the source. However, their existence and separation must be calculated from a single physically specified trajectory rather than introduced as independently adjustable pulse parameters.

The present analysis establishes this mathematical possibility. Quantitative demonstration of multiple GRB peaks requires evaluation of the full arrival-time mapping, including the exact critical

conditions and the emitting region's spatial and temporal structure.

6.5. Finite Emitting Regions and Observable Pulse Width

The temporal-caustic profiles calculated in the preceding sections refer initially to an idealized point-like source. A physical gamma-emitting region has finite dimensions and may contain plasma elements with different positions, radial velocities, accelerations, and emission histories. These differences can broaden the received pulse and reduce its peak intensity.

In the revised source model, the emitting region is a localized volume of magnetized plasma within a larger astronomical environment. It is not required to coincide with the surface of a neutron star. Only the radiation contributing to a particular observed concentration event must possess sufficiently compatible arrival-time histories.

Let x label a position within the emitting region and t_e the local emission time. Under the source-dependent propagation assumption adopted from Part C2, the arrival-time mapping is

$$t_p(t_e, x) = t_e + D(t_e, x)/v(t_e, x),$$

where D is the distance from the emission point to the observer and v is the effective propagation velocity assigned to the outgoing electromagnetic structure in the observer's reference frame. In the simplest version of the model, v = c + u, with u the radial velocity of the emitter toward the observer. If local wave merging modifies that velocity, v must instead represent the outgoing value after this reorganization; the two definitions cannot be interchanged without further justification.

Two distinct sources of arrival-time dispersion can be distinguished. First, simultaneous emissions from positions separated by a line-of-sight depth L‖ have a purely geometric spread, approximately

$$\Delta t_g eom \approx L \parallel /c (v \approx c).$$

This term depends on depth along the line of sight, not on the full transverse diameter of the region. Transverse extent becomes relevant through viewing geometry, internal motions, and correlations between emission positions and times.

Second, if two structures travel approximately the same distance D but have a small difference Δv in their effective propagation velocities, their arrival-time separation is approximately

$$|\Delta t_v el| \approx (D/v^2)|\Delta v| \approx (D/c^2)|\Delta v|.$$

At an illustrative distance of 2.1 billion light-years, limiting this isolated velocity-induced spread to three seconds gives

$$|\Delta v| \lesssim 1.36 \times 10^{-8} ms^{-1}.$$

This is an extremely restrictive tolerance. It applies only to the differential velocity contribution when emission times and distances are held fixed. It is not a universal condition on every plasma element: correlated differences in emission time, location, and effective velocity may compensate one another in the complete arrival-time mapping.

For a source with finite extent, the observed light curve must be constructed by integrating contributions over the emitting region and its emission history. Schematically, for independently averaged contributions,

$$L_p(t_p) = \int d^3x \int dt_e \, L_e(t_e, x) \delta[t_p - g(t_e, x)],$$

where $g(t_e, x)$ denotes the arrival-time map and L_e is an appropriately normalized emission-power density for the selected beam. This expression assumes that different contributions may be added as energies. Coherent overlap requires the electromagnetic fields to be combined before the Poynting flux is evaluated.

The ideal point-source caustic is therefore regularized by the distribution of arrival times across the physical region. A narrow observed pulse requires that a sufficiently energetic subset of the emission occupy a correspondingly narrow range of arrival times,

rather than that the entire surrounding plasma environment move uniformly.

Part B2 proposes that compatible electromagnetic waves may undergo local structural merging and adjustment of their effective propagation velocities. This could reduce part of the initial velocity dispersion before long-distance propagation. However, the degree of synchronization achievable through such merging has not been calculated and must not be assumed to satisfy the numerical tolerance above automatically.

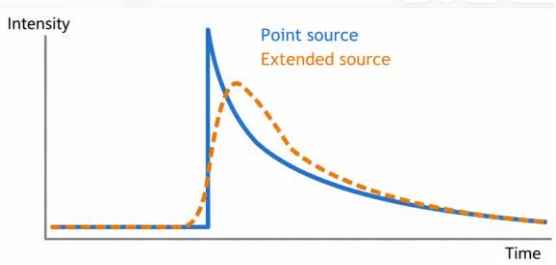


Figure 2. *Schematic comparison of temporal intensity profiles from a point source and an extended emitting region. The finite spatial extent of the source smooths the sharp intensity maximum and broadens the observed pulse while preserving the total received energy under ideal loss-free conditions.*

The finite-region model also permits distinct plasma zones to generate different temporal components. Regions satisfying a near-critical arrival-time condition can contribute a sharp gamma-ray maximum, whereas zones with broader spatial, velocity, or acceleration distributions may produce less concentrated emission.

The present treatment establishes the relevant broadening mechanisms but does not provide a quantitative prediction of the emitting region's allowable dimensions or its complete pulse profile. Those quantities require a specified spatial geometry, a dynamically constrained velocity field, an emission history, and an explicit propagation model. The idealized calculations in Section 5 should therefore be interpreted as limiting cases against which extended-source models can be tested.

6.6. Broader Components and Spectral Evolution

The temporal concentration derived in Sections 3–6 applies to electromagnetic radiation whose emission positions, effective propagation velocities, and source-motion histories produce a sufficiently narrow interval of arrival times. An extended astronomical environment, however, need not satisfy this condition everywhere.

The revised source model considers a number of localized emitting regions embedded in magnetized plasma. These regions may differ in position, gamma-ray luminosity, magnetic-field configuration, radial velocity, acceleration, and intrinsic spectral distribution. Only a subset of their radiation may undergo strong temporal concentration. Other regions may contribute a broader, less intense signal before, during, or after the principal gamma-ray maximum.

Let i identify an emitting region, and let t_e denote the emission time in the observation frame used for the arrival-time calculation. In the source-dependent propagation model, the arrival time of its outgoing radiation is

$$t_{p,i}(t_e) = t_e + D_i(t_e)/v_i(t_e).$$

Here D_i is the distance from region i to the observer at emission, and v_i is the effective outgoing propagation velocity assigned to the relevant electromagnetic structure. In the special case in which the effective velocity follows the local source-dependent relation, $v_i = c + u_i$, with u_i positive for motion toward the observer. If local wave merging changes the outgoing velocity, that effective velocity must be used instead; it cannot automatically be identified with the plasma velocity.

The local arrival-time gradient is

$$J_i(t_e) = dt_{p,i}/dt_e.$$

A region for which $|J_i|$ becomes very small can produce a sharply concentrated received component. Other regions, with different arrival-time mappings or broader distributions of outgoing velocities, need not reach the same critical condition. Consequently, the overall observed light curve may contain a narrow principal peak superimposed on temporally extended emission.

Different emitting regions may also produce different intrinsic spectra. For example, the region responsible for the main temporal concentration may emit predominantly gamma radiation, whereas surrounding plasma regions may contribute additional gamma-ray, X-ray, optical, or radio components. Their emission mechanisms and available powers must be specified independently; temporal concentration alone does not generate new frequency bands.

For mutually incoherent or suitably averaged contributions, the received spectral signal can be expressed schematically as a sum over regions and over emission-time branches that reach the observer at the same time. Each contribution is weighted by its radiation output, propagation and geometric factors, and the inverse magnitude of its arrival-time gradient. Coherent overlap, by contrast, requires calculation of the combined electromagnetic fields and Poynting flux, as discussed in Part B2.

The relative strengths of the received components may change markedly during a burst. Thus, even if the intrinsic spectrum of each region remains approximately stationary, the total observed spectrum may evolve because the relative contributions of the regions change with observation time. Different frequency bands may also reach their maxima at different times if their dominant emitting regions have different arrival-time histories.

Neither the direction nor the magnitude of such spectral delays follows from the arrival-time gradient alone. Quantitative predictions require the positions, motions, intrinsic spectra, emission intervals, and beam geometries of the contributing regions. Likewise, extended radiation should not automatically be identified with a measured GRB afterglow; explaining observed afterglows requires a separate calculation of their luminosity, temporal decay, and spectral behavior.

The proposed interpretation therefore links a sharp gamma-ray maximum and broader accompanying electromagnetic components to the spatial and dynamical diversity of localized emitting regions, without requiring a compact stellar surface to be the primary gamma-ray source. It remains a conditional extension of the propagation hypothesis, to be tested against time-resolved multi-band observations and the energy budget developed in Section 7.

6.7. Implications for GRB Light-Curve Diversity

The source-dependent propagation model allows different gamma-ray burst profiles to arise from different motion histories and spatial distributions of localized emitting regions. The resulting light curve is governed by the arrival-time mapping of the radiation contributing to the observation, rather than by the instantaneous luminosity history of a single stellar surface.

A single stationary point of the arrival-time mapping may produce a sharply concentrated intensity maximum. Depending on the position of the critical point within the emission interval, the observed profile may exhibit a rapid rise, a rapid decline, or an asymmetric combination of both. The idealized mathematical caustic has a finite integrated energy, whereas its measurable peak is limited by the finite size and temporal structure of the emitting region.

When the arrival-time mapping contains two or more stationary points, multiple intensity maxima may occur. Their observed separation and relative strengths depend on the complete motion of the contributing emitting regions,

the intrinsic emission history, and the overlap of the resulting arrival-time branches. Multiple observed peaks therefore need not imply separate short-lived energy-release events, although this interpretation requires quantitative confirmation for a specified source configuration.

The finite dimensions of a magnetized-plasma emitting region modify the idealized profile. Differences in line-of-sight position, effective propagation velocity, and radial acceleration may broaden or displace the received signal. In the proposed model, strong temporal concentration is possible only for the subset of radiation whose complete arrival-time histories remain sufficiently compatible; uniform motion of an entire plasma environment is not required.

Other emitting regions within the same astronomical environment may follow different trajectories and possess different intrinsic spectra. Their radiation may therefore form broader, weaker components before, during, or after the principal gamma-ray maximum. Changes in the relative contributions of these components can produce an evolving observed spectrum, without requiring temporal compression alone to alter the intrinsic spectrum of each electromagnetic structure.

Local electromagnetic interactions and the possible structural merging of compatible waves, discussed in Part B2, may influence the distribution of outgoing propagation velocities. However, the proposed energy-weighted adjustment rule has not yet been shown to generate the exceptionally small velocity dispersion needed for a sharply concentrated burst over cosmological distances. This remains a separate quantitative constraint on the source model.

Consequently, the model permits isolated sharp peaks, multiple maxima, asymmetric pulses, and broader accompanying emission within a common arrival-time framework. Reproducing a measured GRB light curve, however, requires a specified source trajectory, the spatial and spectral distribution of its emission, and a consistent electromagnetic energy balance. These are conditional model possibilities, not yet demonstrated matches to the observed population of gamma-ray bursts [3], [11]

7. Electromagnetic Energy Balance

7.1. Energy Conservation and Temporal Redistribution

The proposed temporal-concentration mechanism changes the distribution of electromagnetic energy in arrival time. It does not, by itself, generate additional energy. For an idealized isolated radiation system, total energy is conserved, but every energy balance must be expressed in a specified observation frame.

Let K denote a single reference frame in which the emitted radiation, its propagation, and the receiving surface are described. For a selected radiation bundle that retains all its energy during propagation, the integral balance is

$$W_{\mathrm{re}}{}^{(\mathrm{K})} = W_{\mathrm{em}}{}^{(\mathrm{K})}.$$

If radiation is lost from that bundle through absorption, scattering, or transport into other directions, the retained fraction may be represented by η, with $0 \le \eta \le 1$:

$$W_{\mathrm{re}}{}^{(\mathrm{K})} = \eta W_{\mathrm{em}}{}^{(\mathrm{K})}.$$

This expression refers to the same bundle and the same observation frame. It is not an assertion that the energy assigned to an electromagnetic structure in the rest frame of its source is numerically identical to the energy assigned to that structure in the Earth-based frame.

In particular, let K_S be the local source frame and K_Z the receiver frame. The model permits the possibility that the energies assigned to a

propagating electromagnetic structure differ between these frames:

$$W^{(z)} \neq W^{(s)}.$$

Part B2 discusses a proposed frame-dependent energy relation for such structures. However, a validated transformation law between $W^{(s)}$ and $W^{(z)}$ has not yet been established. The present section therefore makes no numerical identification between them. The energy redistribution calculated below is formulated entirely in the receiver frame K_Z.

Temporal concentration increases the rate at which a given bundle delivers energy to the receiver, while leaving its time-integrated received energy unchanged under the stated idealization. Geometrical spreading and detector interception must be treated separately: a detector generally receives only a fraction of the energy carried by the full astronomical emission.

7.2. Energy Transport Through the Arrival-Time Mapping

Let t_e be the emission-time coordinate and t_p the arrival-time coordinate, both referred to the chosen receiver-based description K_Z. The source-dependent propagation hypothesis of Part C2 specifies an arrival-time mapping

$$t_p = g(t_e), J(t_e) = dt_p/dt_e.$$

Define $L_e^{(z)}(t_e)$ as the energy emitted per unit t_e into the selected bundle, with that energy evaluated in K_Z. Let $\eta(t_e)$ represent the fraction subsequently retained in the same bundle. For an interval on which g is monotonic, the receiver-frame energy balance is

$$\begin{aligned} dW_{rec}^{(z)} &= \eta(t_e)\, L_e^{(z)}(t_e)\, dt_e \\ &= L_p^{(z)}(t_p)\, |dt_p|. \end{aligned}$$

Consequently, the received equivalent beam power is

$$L_p^{(z)}(t_p) = \eta(t_e) L_e^{(z)}(t_e)/|J(t_e)|.$$

When several emission times $t_{e,i}$ correspond to the same arrival time t_p, their independently averaged energy contributions are summed:

$$L_p^{(z)}(t_p) = \Sigma_i\left[\eta(t_{e,i}) L_e^{(z)}(t_{e,i})/|J(t_{e,i})|\right].$$

The absolute value of J is necessary on branches where the ordering of arrivals is reversed. The formula describes an incoherent or suitably averaged energy-transport envelope. If the arriving electromagnetic structures remain mutually coherent, their electric and magnetic fields must be combined before the resulting Poynting flux is calculated, as discussed in Part B2.

Integrating over the complete arrival interval, counting each contributing emission branch once, gives

$$\int L_p^{(z)}(t_p) dt_p = \int \eta(t_e) L_e^{(z)}(t_e) dt_e.$$

For ideal loss-free transport, $\eta = 1$, and the right-hand side equals the receiver-frame energy assigned to the emitted radiation bundle. Thus a large, even formally divergent, value of the idealized power near J = 0 does not imply an infinite or newly created total energy.

The calculation does not establish the source-to-receiver energy transformation. If source-frame luminosity $L_e^{(s)}$ is used instead, a separate transformation of energy and emission-time coordinates is required before it can be inserted into the receiver-frame balance. The timing Jacobian alone is not such a transformation.

The resulting power enhancement remains conditional on the source-dependent propagation law, the assumed conservation of energy within the followed bundle, and the physical realization of the electromagnetic fields at the temporal caustic.

7.3. The Thirty-Day Example and Its Energy Budget

The gravitational example developed in Section 5 describes a localized gamma-emitting region whose radiation, emitted continuously over thirty days, reaches the observer within approximately three seconds under the proposed source-dependent propagation relation.

The corresponding mean temporal concentration factor is

$$\bar{K} = T_e/T_p = 2{,}592{,}000/3 = 864{,}000.$$

To evaluate the energy balance consistently, all energies and powers in this example are assigned to the observation frame KZ, in which the receiving observer is at rest. The emission interval T_e is the interval between emission events expressed in this frame; it is not automatically identical to an interval measured by a moving source clock.

Let $L_e(Z)$ denote the equivalent electromagnetic power assigned to the selected radiation beam in this observation frame. For constant power over the specified emission interval, the corresponding beam energy is

$$W_e(Z) = L_e(Z)T_e.$$

If the energy in this beam remains unchanged during propagation and the beam geometry is treated separately, its mean equivalent received power is

$$L_p(Z) = W_e(Z) / T_p = K\, L_e(Z).$$

As a deliberately illustrative normalization, assume

$$L_e(Z) = 10^{32}W.$$

The energy assigned to thirty days of emission is then

$$W_e(Z) = 10^{32} \times 2{,}592{,}000 = 2.592 \times 10^{38}J.$$

Concentrating the same beam energy into three seconds gives

$$\bar{L}_p(Z) = 2.592 \times 10^{38}/3 = 8.64 \times 10^{37}W.$$

The assumed luminosity is an illustrative model input, not a measured gamma-ray luminosity of a neutron-star surface or of any particular plasma region.

Quantity	Before temporal concentration	After temporal concentration
Time interval	30 days	3 s
Mean equivalent beam power in KZ	$L_e(Z)$	864,000 $L_e(Z)$
Beam energy in KZ	$L_e(Z)\, T_e$	$L_e(Z)\, T_e$
Energy-retention factor	$\eta = 1$	$\eta = 1$

***Table 3**. Integral energy accounting for an idealized single-beam, loss-free temporal concentration. Temporal concentration changes power and duration, not the total beam energy.*

Temporal concentration changes the time distribution and mean equivalent power of a selected radiation beam, not its total energy in the specified frame. The actual detector flux additionally depends on the beam solid angle, distance, collecting area, and attenuation. The numerical concentration factor does not establish that the emitting region can physically supply the assumed gamma-ray power.

If source-frame energy differs from energy attributed to the same radiation in the observer frame, a separate transformation law is required before these quantities can be compared. Such a law is not derived here. The present example establishes an energy-accounting condition within KZ, conditional on the assumed propagation relation and idealized conservation of the followed beam energy.

7.4. Local Conservation and the Poynting Vector

The integral balance is consistent with local electromagnetic energy conservation only if the underlying fields and energy flux satisfy the Poynting theorem. In vacuum, the standard electromagnetic energy density and Poynting vector are

$$w = \frac{\varepsilon_0 E^2}{2} + \frac{B^2}{2\mu_0}$$

$$\vec{S} = \frac{\vec{E} \times \vec{B}}{\mu_0}$$

Their local continuity equation is

$$\partial w/\partial t + \nabla \cdot \vec{S} = -\vec{J} \cdot \vec{E}$$

In a source-free propagation region where the current density vanishes, the right-hand side is zero. For any fixed volume, the change of stored electromagnetic energy is therefore balanced by the net energy flow through its boundary.

A rise in detected flux can consequently be consistent with energy conservation when the spatial and temporal arrangement of incoming radiation produces a correspondingly increased flux through the receiving surface. The continuity equation does not, by itself, derive the assumed c + u arrival-time law or specify the detailed field configuration at a temporal caustic.

For a single approximately plane, propagating wave, the time-averaged Poynting flux is related to the wave amplitude. If the propagation impedance and effective transport speed are unchanged, an ideal intensity concentration by $\bar{K}$ would correspond to a characteristic field-amplitude factor of $\sqrt{\bar{K}}$, about 930 for the thirty-day example. This is a conditional scaling for an equivalent combined field, not a prediction that the field amplitude of every individual arriving wave increases by that amount.

$$S_p/S_0 = K, \quad E_eff,p/E_eff,0 \approx \sqrt{K}$$

7.5. Overlap, Coherence, and Electromagnetic Structure

The previous sections of the research programme address coherent electromagnetic structures rather than introducing a photon-counting description. Part B2 develops the conditions under which neighbouring electromagnetic waves or coherent chains may connect and alter their geometry during propagation. The characteristic radius R and chain length L may increase when the stated coherence and compatibility requirements are satisfied.

The present GRB calculation does not require every approaching pair of waves to merge. Temporal concentration and coherent merging are distinct processes: the former concerns the arrival times of transported energy, whereas the latter concerns the spatial organization of the electromagnetic structures carrying that energy.

An ideal coherent-merging process without losses preserves the sum of the incoming energies:

$$W_after = \Sigma_i W_before,i$$

If part of the energy is redirected or radiated into other modes, total conservation requires

$$\Sigma_i W_before,i = W_after + W_other$$

A merged structure may therefore possess greater individual energy and modified R or L without implying any increase in the total energy of the original set of waves. These conditions are taken from the earlier model and are not re-derived here.

When several coherent fields overlap at the receiver, the local Poynting vector must be computed from the total fields:

$$\vec{E}_{tot} = \Sigma_i \vec{E}_i, \quad \vec{B}_{tot} = \Sigma_i \vec{B}_i$$

$$\vec{S}_{tot} = \frac{\vec{E}_{tot} \times \vec{B}_{tot}}{\mu_0}$$

Consequently, field interference, coherent merging, and statistical averaging must not be conflated with simple addition of intensities. The power-summation formula in Section 7.2 describes an energy-transport envelope; detailed interference structure belongs to the electromagnetic modelling developed in Part B2.

7.6. Source Luminosity, Beaming, and the Observed Fluence

The ability of temporal concentration to generate a large peak power must be distinguished from the ability of the source to supply the energy measured in a GRB. Let W_{iso} denote the isotropic-equivalent emitted energy and D_L the luminosity distance used in the observational energy conversion. For an event at cosmological redshift z, the commonly used bolometric relation is

$$Wiso = \frac{4\pi D_L^2 F}{1 + z}$$

where F is the observed fluence integrated over a specified energy range with the appropriate spectral correction. In a local, non-cosmological approximation, the relation reduces to $W_{iso} \approx 4\pi D^2 F$. A strongly beamed source may require less actual emitted energy than its isotropic equivalent.

Temporal concentration changes the received time profile and peak flux, but it does not by itself increase the observed fluence. The amplitude of the burst is therefore controlled jointly by the energy available at the source, the portion emitted toward the observer, propagation losses, and the arrival-time concentration factor.

7.7. Energy-Balance Result and Scope

The mathematical result of this section is that the proposed arrival-time mapping can redistribute a finite emitted electromagnetic energy into a short observer interval while preserving its integral. In the thirty-day example, the mean equivalent beam power rises by a factor of 864,000 solely because the arrival interval is reduced to three seconds.

This result is conditional on the adopted propagation model and the conservation of energy in the followed beam. The Poynting theorem supplies the local conservation requirement, while the coherent-merging conditions and structural changes of electromagnetic chains are addressed separately in Part B2. Neither the arrival-time Jacobian nor the integral equality alone constitutes a complete field solution at the caustic.

Accordingly, the energy balance establishes a consistency condition for the temporal-concentration hypothesis, not an independent demonstration that astrophysical GRBs are produced in this manner. The spectral components and accompanying radiation considered next provide further observational tests of the proposed source model.

8. Spectral Evolution and Afterglow

8.1. Distinct Emission Regions and Their Observed Contributions

The temporal-concentration model developed in Sections 3–7 describes the observed gamma-ray burst as a redistribution of the arrival times of electromagnetic energy emitted by a moving compact source. The present section examines whether the same

framework can also accommodate spectral evolution and radiation observed before or after the main burst. These phenomena are treated as possible contributions from physically distinct emission regions, not as consequences that automatically follow from temporal compression alone.

The model distinguishes a localized region of magnetized plasma whose radiation may undergo strong temporal concentration from other emitting zones in the surrounding astronomical environment. The participating region must have sufficiently compatible emission positions, effective propagation velocities and arrival-time histories. Other regions can have different local motions, accelerations and spectra, producing broader temporal components. The existence of a sufficiently energetic and suitably synchronized gamma-emitting region remains a source-model requirement to be verified quantitatively; direct radiation from a neutron-star surface is not assumed.

The model makes no requirement that all gamma-ray bursts have the same intrinsic spectrum or that every afterglow have a single physical origin. It asks whether a compact component and one or more extended components can jointly account for part of the observed time-dependent spectrum.

8.2. Spectral Transport Through the Arrival-Time Mapping

Let i label an emitting region. Its emission and arrival times are related, in the source-dependent propagation model adopted from Part C2, by

$$t_{p,i} = t_e + \frac{D_i(t_e)}{c + u_i(t_e)}$$

The local arrival-time Jacobian is

$$J_i(t_e) = \frac{dt_{p,i}}{dt_e}$$

Let $L_{e,i}(f, t_e)$ be its spectral luminosity per unit frequency and unit emission time. Subject to energy conservation within the selected radiation beam, fixed propagation factors across the interval, and an incoherent or suitably averaged sum of components, the received spectral flux density is

$$F_p(f, t_p) = \sum_i A_i \sum_k \frac{L_{e,i}(f, t_{e,i,k})}{|J_i(t_{e,i,k})|}$$

Here A_i accounts for geometric dilution, directional emission, and any specified attenuation, while k enumerates all emission times mapped to the same observer time. Under the working assumption of frequency preservation for individual electromagnetic structures, the same frequency argument f appears on both sides. The treatment of coherent overlap requires the total electromagnetic fields, rather than an unconditional sum of separate intensities, as discussed in Section 7 and Part B2.

If the emitting spectrum has a time-independent shape,

$$L_{e,i}(f, t_e) = P_i(t_e)\, \Phi_i(f)$$

then temporal compression changes its amplitude but does not, by itself, alter the normalized spectral shape $\Phi_i(f)$. Consequently, a change in the measured spectrum requires differing component spectra, intrinsically evolving emission, frequency-dependent selection, or additional propagation processes. This is an important limitation and testable prediction of the proposed mechanism.

8.3. The Main Gamma-Ray Peak

Near a critical arrival time of the localized gamma-emitting component S, the Jacobian approaches zero,

$$J_S(t_{e,0}) = 0$$

and the received gamma-ray flux can become strongly concentrated. For a locally quadratic mapping, the idealized one-branch enhancement derived in Section 6 follows

$$F_{p,S}(f, t_p) \propto \frac{\Phi_S(f)}{\sqrt{|t_p - t_{p,0}|}}$$

within the local approximation and away from physical regularization scales. This expression refers to the time dependence of the flux at a specified frequency; it does not imply that the gamma-ray spectrum is necessarily narrow in frequency. A narrow time profile and a narrow spectral distribution are different properties.

If the localized gamma-emitting region dominates the peak, its intrinsic spectrum should largely determine the observed peak spectrum, subject to the propagation assumptions and instrumental response. Radiation from other plasma zones may contribute broader, less concentrated components. In this framework, the principal burst reflects a change in the arrival rate of electromagnetic energy rather than necessarily a sudden increase in intrinsic source power.

8.4. Extended Plasma-Region Emission

Let h denote the line-of-sight depth of an extended plasma emitting region. Its purely geometrical arrival-time spread is approximately

$$\Delta t_{\mathrm{geom}} \simeq \frac{h}{c}$$

For an illustrative depth of $3000\ \mathrm{km}$, this gives only about $0.010\ \mathrm{s}$. The corresponding spread across a stellar diameter of $24\ \mathrm{km}$ is about $8.0 \times 10^{-5}\ \mathrm{s}$. Thus depth alone is not sufficient to explain an afterglow lasting hours or days.

Within the adopted propagation relation, additional dispersion of arrival times can arise from differences in line-of-sight velocity between emitting structures. For small differences at a common distance D,

$$\Delta t_u \simeq \frac{D}{c^2}|\Delta u|$$

At $D = 2.1 \times 10^9$ light-years, a difference $|\Delta u| = 10^{-8}\ \mathrm{m\,s^{-1}}$ corresponds formally to an arrival-time separation of approximately $2.2\ \mathrm{s}$. This sensitivity motivates a broader signal from other plasma regions, but the estimate compares simultaneous emissions; it is not by itself a calculated full afterglow light curve. A physically predictive result requires specified emission sites, their dynamical histories, and the duration of their intrinsic radiation.

Other plasma regions may also produce X-ray, optical, or radio emission. The emitted frequency bands and their powers require a physical radiation model and cannot be inferred from the time-of-flight transformation alone.

8.5. Spectral Evolution and Delays Between Energy Bands

Suppose the localized gamma-emitting component has spectrum $\Phi_S(f)$ and an extended region has a different spectrum $\Phi_M(f)$. The time-dependent observed spectrum can be written schematically as

$$F_p(f, t_p) = K_S(t_p)\Phi_S(f) + K_M(t_p)\Phi_M(f)$$

The coefficients K_S and K_M represent the received contributions after the respective arrival-time transformations, including their normalizations. Even if both intrinsic spectral shapes are constant, their changing relative weights can produce an evolving combined spectrum. For example, the central gamma-ray peak can be dominated by the compact component,

whereas softer radiation may become relatively more important on either side of the peak.

Different frequency bands need not reach their maximum at the same time if they are dominated by different emitting regions. Denoting two observed bands by γ and X,

$$\Delta t_{X\gamma} = t_{p,X}^{\max} - t_{p,\gamma}^{\max}$$

A difference in the derivatives $j_i = da_i/dt_e$ influences the widths and curvatures of the time mappings; it does not alone establish the sign or magnitude of $\Delta t_{X\gamma}$. Those depend on the positions of the critical times, the complete motions, and the histories of the respective emitting regions. The theory therefore accommodates possible time lags as a hypothesis, but requires quantitative modeling before specific lag patterns can be claimed.

8.6. Afterglow and Long-Term Evolution

Observed GRB afterglows may extend into X-ray, optical, and radio bands far beyond the prompt gamma-ray signal. In the proposed multi-region interpretation, radiation from plasma zones with different motion and emission histories could contribute to longer-lived components. A localized region satisfying the near-critical condition may produce a sharp gamma-ray peak, whereas other regions with broader arrival-time mappings may produce a weaker temporal envelope.

Nevertheless, a long afterglow cannot be attributed to geometrical depth alone. For durations of days or weeks, the source must supply an adequate amount of electromagnetic energy and a motion/emission history that maps it into the corresponding observer-time interval. Spectral evolution and declining luminosity must then be calculated, not merely associated with an extended region. Established afterglow phenomenology also includes external-shock emission; any proposed alternative must ultimately be compared against measured multi-band temporal and spectral behavior.

An informative test would be whether a single dynamically constrained source geometry can reproduce both the prompt gamma-ray peak and the later emission without independently assigning arbitrary time profiles to each band. A second test concerns the integrated energy of each component, which must remain consistent with the conservation framework developed in Section 7.

8.7. Observational Consequences and Scope

The localized-region picture suggests several observational checks. First, the principal gamma-ray peak should be narrower than surrounding emission when its contributing radiation has more tightly grouped arrival-time histories. Second, its spectrum should reflect that of the dominant emitting region, while evolution outside the peak may reveal changing contributions from other zones. Third, cross-band delays should follow from the complete calculated mappings and emission histories of those zones, rather than from temporal compression alone. Finally, their energy supplies and directional emission must account for the integrated energy of the whole event.

These are conditional consequences of the proposed source-dependent propagation model, not established explanations of observed GRB afterglows. The revised model does not require gamma emission from a stellar surface or negligible neutron-star rotation. Quantitative predictions still require a physically specified emitting-region geometry, energy supply, and motion history. the planned companion study on pulsar dynamics. The present

section establishes a calculable framework for spectral superposition and time lags while identifying the information needed for a quantitative comparison with GRB observations. [9], [10], [11]

9. Observational Implications

9.1. Connecting the Proposed Mechanism with GRB Observations

The preceding sections establish a conditional prediction of the proposed source-dependent propagation model: a compact gamma-emitting source undergoing suitable gravitational motion may produce a short and intense arrival-time concentration of radiation emitted over a much longer interval. The model must nevertheless be assessed against the observed population of gamma-ray bursts rather than against the time profile of a single selected event.

GRBs exhibit a wide diversity of durations, peak intensities, pulse structures, spectral hardness, time lags, fluences, and accompanying emission. The Fermi Gamma-ray Burst Monitor (GBM) catalogues provide distributions of these quantities, while follow-up observations identify host galaxies and, for some events, associated supernovae or compact-object mergers. These are independent observational constraints, not interchangeable measurements of the same physical mechanism.

The purpose of this section is to distinguish three levels of agreement: (i) effects derived quantitatively from the arrival-time mapping; (ii) behaviours that the model allows only after introducing source or magnetospheric structure; and (iii) observations for which the present model has not yet supplied a quantitative explanation.

9.2. Burst Duration and Temporal Diversity

An observational distinction is commonly made between short and long GRBs using a duration near two seconds, although the two populations overlap and duration alone does not uniquely identify the progenitor. Individual bursts range from sub-second events to long and complex emission episodes (Fermi GBM burst catalogues).

Within the proposed model, the primary observable is not the intrinsic emission duration of the localized gamma-emitting region, but the interval into which its radiation is mapped at Earth. Near a critical emission time t_o, a locally quadratic mapping gives

$$t_p - t_{p,0} \approx A(t_e - t_0)^2$$
$$T_p \approx |A| {T_e}^2$$

For a short interval and small radial speed, the coefficient is approximately related to the radial acceleration gradient j and propagation distance D:

$$|A| \approx \frac{|j|D}{2c^2}$$

Consequently, duration depends on the combination of source-motion history, distance, and the interval over which emission is present. Sections 4 and 5 demonstrate illustrative gravitational examples in which one hour, one day, or thirty days of radiation are mapped into intervals of a few seconds. These are model calculations, not fits to the observed distribution of GRB durations.

Different configurations may also lead to isolated pulses, multiple arrival-time branches, or broader emission around a caustic. The range of observed temporal profiles is therefore qualitatively compatible with a family of different

source trajectories, but reproducing the actual population requires a statistical distribution of source masses, orbital parameters, viewing directions, emitting-region sizes, and intrinsic emission histories.

9.3. Peak Flux, Fluence, and the Energy Range

The arrival-time Jacobian predicts that a short receiving interval can have a much higher mean energy flux than the same beam would have without temporal concentration. For a single monotonic branch with retained energy fraction η, the schematic relation is

$$L_{\mathrm{p}}(t_{\mathrm{p}}) = \frac{\eta L_{\mathrm{e}}(t_{\mathrm{e}})}{|dt_{\mathrm{p}}/dt_{\mathrm{e}}|}$$

For approximately constant source power, an emission interval T_e mapped into an observed interval T_p has mean concentration factor

$$K = \frac{T_{\mathrm{e}}}{T_{\mathrm{p}}}$$

The thirty-day numerical example gives $\bar{K}$ = 864,000 for a three-second receiving interval. This factor applies to mean power in the followed beam, not to its total energy. Conservation of the transported energy requires the time-integrated receiving flux to remain fixed for the chosen emission interval, apart from propagation losses and geometric dilution.

Observational fluence and inferred isotropic-equivalent energy vary greatly across the GRB population. The model allows such diversity through source luminosity, emission duration, radiation directionality, propagation distance, and temporal concentration. It does not predict the absolute fluence of a particular GRB unless the intrinsic gamma-ray output and beaming geometry are independently constrained.

A crucial distinction is therefore maintained: temporal concentration may explain a high peak flux relative to a persistent source, whereas the integrated energy of a very energetic event must still be supplied by the source. The required gamma-ray luminosity of a localized plasma region must be justified by a physically available energy reservoir and transport mechanism, rather than inferred from burst intensity alone.

9.4. Spectral Hardness and Energy-Dependent Time Lags

Fermi GBM measurements show that short and long GRBs have different statistical hardness distributions, and time-resolved spectra frequently evolve during a burst. Spectral lags between energy bands have also been measured in many bright pulses (Nava et al., 2011; Lu et al., 2018).

A pure arrival-time concentration of radiation from one emitting region, with a stationary intrinsic spectrum and a frequency-independent mapping, changes the overall amplitude but does not by itself change the relative spectral shape. For one such region the predicted observed spectral energy flux can be written

$$F_{\mathrm{p}}(f, t_{\mathrm{p}}) = K(t_{\mathrm{p}})\Phi_{\mathrm{e}}(f)$$

Accordingly, spectral evolution and delays cannot be attributed to a single common multiplier $K(t_p)$. The multi-region hypothesis developed in Section 8 allows the sharp gamma-ray maximum to be dominated by one localized emitting zone, while other plasma zones contribute components with different radial motions, arrival-time mappings, and intrinsic spectra.

$$F_{\mathrm{p}}(f, t_{\mathrm{p}}) = K_S(t_{\mathrm{p}})\Phi_S(f) + K_M(t_{\mathrm{p}})\Phi_M(f)$$

This expression predicts that the spectrum can change as the relative contribution of

the two regions changes. It also allows the maxima in different energy bands to be displaced when the corresponding bands are dominated by different emission zones. However, neither the sign nor the magnitude of a spectral lag follows from the difference in j alone: these require the positions, velocity histories, intrinsic spectra, and emission times of the contributing regions.

A directly testable consequence is that spectral changes should correlate with the evolving mixture of the temporal components. Whether the resulting evolution agrees with observed hard-to-soft trends or pulse-to-pulse spectral behaviour remains to be calculated.

9.5. Extended Emission and Afterglow

Many GRBs are followed by X-ray, optical, and sometimes radio emission extending well beyond the prompt gamma-ray phase. Such afterglows provide information about the emitting environment and, in established interpretations, about interactions with surrounding material.

In the present proposal, different emitting zones of a magnetized plasma environment need not share the sharply concentrated arrival-time mapping of the zone responsible for the principal peak. Their radiation may therefore contribute lower-contrast, longer-lived components preceding or following the main caustic.

This possibility is distinct from a derived explanation of the full afterglow phenomenology. The current model has not yet reproduced measured multi-band decay indices, evolving spectral breaks, or the radio evolution of afterglows. These observables should be treated as quantitative tests for a future detailed model of magnetospheric emission.

The association of certain long GRBs with supernovae and the joint detection of GRB 170817A with the gravitational-wave source GW170817 and a kilonova also constrain the underlying astrophysical event. A propagation-based explanation of the prompt light curve must be assessed together with these independent observations; their existence cannot be established or negated by arrival-time compression alone.

9.6. Proposed Observational Tests

The following comparisons would distinguish a purely temporal-concentration hypothesis from broader source models and from competing interpretations. They are presented as research tests rather than claimed confirmations.

Observable	Specific model implication	Present status
Pulse width and shape	Near a quadratic caustic, a sharp, integrable peak; width depends on j and emitting interval.	Calculated for idealized examples
Peak flux versus fluence	Strong peak enhancement without proportional increase of integrated beam energy.	Conditional energy accounting
Within-peak spectral shape	Single-zone compression alone preserves a fixed intrinsic spectral shape.	Directly testable; not generally sufficient

Energy-band lags	Different emission regions may show distinct peak arrival times.	Requires a multi-region calculation
Afterglow duration	Extended magnetospheric emission may be less concentrated than surface emission.	Qualitative hypothesis
Pre-burst persistent source	The emitter may radiate outside the observed caustic interval.	Search limited by instrumental sensitivity and source distance
Host and counterpart evidence	Compact-source motion must remain consistent with observed host, supernova, or merger associations.	Unresolved for individual GRBs

***Table 4**. Selected observational discriminants for the proposed temporal-concentration mechanism. The status column deliberately distinguishes mathematical results from qualitative expectations and unresolved physical requirements.*

A particularly useful comparison would combine a high-time-resolution gamma-ray light curve with time-resolved spectral measurements and an independently determined source distance. The model would then have to predict the pulse profile and the evolution of its spectral components using the same source-motion parameters, rather than tuning a separate temporal mapping for each observable.

9.7. Scope of the Observational Comparison

The proposed mechanism offers a quantitative explanation for how a short receiving interval may arise from a much longer emission interval, conditional on the source-dependent propagation relation adopted from Part C2. Natural gravitational motion supplies explicit examples of the required radial acceleration and acceleration gradient. The associated mean-flux amplification and finite energy integral are derived in Sections 6 and 7.

Thus, the observational case for the temporal-concentration model should presently be described as a set of specific, potentially falsifiable predictions rather than as a demonstrated alternative explanation of all GRBs. The combined timing, spectral, energy, and counterpart constraints provide the basis for the broader discussion in Section 10. [3], [4], [5], [11]

10. Discussion

10.1. A Unified Interpretation of Temporal Concentration

The calculations developed in the preceding sections suggest a coherent way to investigate gamma-ray bursts as a propagation-time phenomenon. A compact source may emit gamma radiation over a substantial interval while its gravitational motion continuously changes the arrival-time distribution. Within the source-dependent propagation hypothesis adopted from Part C2, the observed high-intensity event can

therefore differ greatly in duration and peak flux from the underlying emission process.

An important outcome is that the model does not require a universal source mass, orbit, luminosity, or emission duration. The critical condition identifies a class of favorable configurations, while the distribution of radial accelerations and their temporal gradients across astronomical systems naturally allows a diversity of pulse profiles. The mechanism is thus formulated as a common physical principle rather than as a reconstruction tailored to one observed GRB.

This distinction suggests a useful direction for future work: observed burst populations can be analyzed in terms of their arrival-time geometry without assuming beforehand that every event must share the same detailed source history. The present results establish the mathematical consequences of the proposed propagation relation; whether that relation describes astronomical light is a separate empirical question addressed by the associated work.

10.2. Gravitational Motion as a Source of Diverse Burst Durations

The binary examples demonstrate how different emission intervals can be mapped into similarly short receiving intervals by ordinary gravitational motion. In the illustrative 1.4- and 1.0-solar-mass system, changing the orbital separation modifies the line-of-sight acceleration and its gradient without introducing an arbitrarily chosen acceleration function. The examples span an hour, a day, and thirty days of emission, each producing a receiving interval of only a few seconds under its specified critical geometry.

The governing local relation is particularly informative: for an emission interval beginning at a critical arrival-time point, and when the quadratic approximation is valid, the observed interval scales with the acceleration gradient and the square of the emission duration.

$$\Delta t_p \simeq \frac{|j|D}{2c^2} T_e^2$$

Consequently, extending the emission period while retaining a short burst requires a sufficiently small effective gradient and sustained proximity to the critical regime. Very long emission intervals also call for evaluation of the full trajectory, since higher-order changes in motion can become significant. This is a promising route for exploring whether days, weeks, or months of emission can contribute to individual observed events; it also provides a concrete criterion for identifying which gravitational systems are capable of such concentration.

The orbital parameters should not be interpreted as unique fits to the GRB population. They are constructive examples showing how the kinematic condition can arise from gravitational equations. Eccentric motion, multi-body systems, and evolving orbital configurations offer further calculable families of source histories.

10.3. Energy Concentration Without Additional Energy Production

The model separates the total energy carried by the radiation from the interval during which that energy is received. For a steadily emitting source, a longer emission interval contains more radiation energy. If the arrival-time mapping compresses this interval, the mean energy flux during the resulting event rises correspondingly, while the integrated energy of the followed beam is conserved under ideal loss-free propagation.

$$\overline{K} = \frac{T_e}{T_p}, \qquad W_{\mathrm{beam},p} = W_{\mathrm{beam},e}$$

For the thirty-day to three-second example, the mean concentration factor is 864,000. This numerical result concerns redistribution in time, not multiplication of the emitted energy. The detected fluence additionally depends on distance, the directional distribution of the radiation, and propagation losses. A broad range of intrinsic source luminosities and durations can therefore yield a broad range of observed peak fluxes and fluences.

The electromagnetic interpretation is consistent with the integral energy-accounting condition only when the proposed wave evolution supplies the corresponding local energy flux. Poynting's theorem provides the local conservation constraint, while the coherent merging and structural evolution of electromagnetic waves are treated separately in Part B2. Such merging may change characteristic dimensions R and L and redistribute energy among structures, without creating net energy in an isolated process.

A useful extension is to calculate the total emission duration and intrinsic luminosity needed for selected fluence ranges, keeping the beaming geometry explicit. That exercise would further connect the arrival-time mechanism with the diversity of observed burst energies, without selecting an exceptionally energetic source as a universal requirement.

10.4. Localized Emission and Extended Surrounding Radiation

A central feature of the revised source model is the distinction between a localized plasma region whose outgoing radiation has sufficiently compatible arrival-time histories and an extended environment containing other radiating regions. The latter can have a wider distribution of emission positions, radial velocities, accelerations, and intrinsic spectra. Its radiation may consequently arrive over a broader interval.

This separation provides a physically interpretable way to examine a sharp gamma-ray maximum accompanied by weaker and longer-lasting radiation. It also allows the observable spectrum to evolve through changing contributions from different emitting regions, without requiring that the frequency of each individual electromagnetic structure change during propagation.

This division is a working source hypothesis. It creates two quantitative tasks: determining whether a localized region can sustain the required gamma-ray output and sufficiently narrow arrival-time distribution, and calculating the other regions needed to reproduce measured multi-band light curves. Neither task is resolved by the idealized point-source caustic calculation.

10.5. Spectral Evolution, Band-Dependent Delays, and Afterglows

The model suggests that spectral diversity can arise not only from different source spectra, but also from different time mappings of distinct emitting regions. A narrow burst dominated by one compact source may have a spectral composition different from the broader emission before and after its maximum. If gamma-ray, X-ray, optical, and radio contributions originate in regions with different kinematic histories, their maxima need not coincide.

A useful observational test is therefore to compare time-resolved spectral changes with the evolution of the narrow and broad temporal components. A common concentration function acting on a single stationary source spectrum would

preserve its relative spectral shape; measurable departures would identify the contribution of additional emitting regions or intrinsic source evolution.

Long-lasting afterglows can be investigated in this framework as a combination of more broadly distributed source emission and propagation-time effects. Existing observations of afterglow spectra, temporal decays, and associations with supernovae or compact-object mergers provide important independent evidence to include in such comparisons. A future treatment should test whether the proposed contribution from other plasma regions reproduces these observations quantitatively, rather than merely resembling their duration.

10.6. Research Opportunities and Predictive Development

The principal opportunity opened by this model is a direct link between calculable source motion and observable time profiles. Rather than adjusting a light curve independently, one can derive the emitting body's trajectory from gravitational dynamics, determine its arrival-time map, and use that map to predict burst duration, pulse shape, and energy concentration. Finite source size and spatially distributed plasma radiation can then be included as physically motivated extensions.

Three complementary lines of development are especially productive. First, extending the numerical calculations to eccentric and evolving orbits would identify the range of natural critical crossings. Second, coupling the arrival-time map to geometrically resolved plasma regions would yield quantitative peak widths and contrasts. Third, joint fits to gamma-ray and lower-energy light curves would test whether their delays and spectral evolution can be attributed to distinct emission regions.

The model also suggests comparative observational tests: events with similar observed durations need not imply similar emission durations; peak flux need not scale directly with source luminosity; and temporally broad accompanying emission may have a distinct spectral origin from the central gamma peak. These propositions are testable only when combined with independent source information or with sufficiently constrained multi-band measurements.

In this perspective, the results of the present study establish a quantitative basis for the temporal-concentration hypothesis and identify specific calculations capable of sharpening it. They provide a foundation for a compact set of falsifiable predictions, to be developed further as the source and propagation models are refined. [1], [2], [7], [8]

11. Conclusions

This study investigates a possible interpretation of gamma-ray bursts (GRBs) as temporal concentrations of electromagnetic radiation emitted over much longer intervals than the observed bursts. Its central premise is the source-dependent propagation hypothesis developed in Part C2. Within that hypothesis, changes in the radial motion of a localized emitting region alter the arrival times of successive electromagnetic structures, potentially concentrating an extended emission history into a short observational interval.

The revised source model does not require gamma radiation to originate from the surface of a non-rotating neutron star. Instead, it considers localized emitting regions within magnetized plasma or related high-energy astronomical environments. A neutron star or binary system may supply gravitational motion, electromagnetic energy, or both, but is not an indispensable direct emitter. The

relevant kinematic quantities are the radial velocity, resultant radial acceleration, and its time derivative for the radiation-contributing region.

The arrival-time transformation yields a critical condition at which its derivative with respect to emission time vanishes. Near such a point, radiation from a range of emission times can become concentrated into a narrow arrival interval. Gravitationally determined binary trajectories provide explicit examples of this effect, while electromagnetic and other forces could contribute to the resultant acceleration in more general plasma environments. Their quantitative effects are not calculated in the present examples.

Three illustrative binary configurations map emission lasting one hour, one day, and thirty days into receiving intervals of a few seconds. The thirty-day example yields a mean temporal concentration factor of 864,000 for a three-second arrival window. These results are conditional calculations within the assumed propagation law; they are not fitted explanations of individual observed GRBs.

The model also permits a range of idealized temporal profiles. A single stationary point can produce a sharp, integrable temporal caustic; multiple stationary points and emission branches may produce more complex structures. The observable peak width and shape additionally depend on the spatial extent, local velocity distribution, and emission history of the participating region. In particular, the extremely small propagation-velocity differences compatible with a seconds-long burst at cosmological distances remain a demanding quantitative constraint.

Part B2 proposes that compatible electromagnetic waves or coherent wave chains may reorganize into common structures and thereby adjust their effective propagation characteristics. Such local merging could contribute to velocity uniformity within an emitting region, but neither the required degree of synchronization nor a complete field-dynamical description has yet been demonstrated. The arrival-time calculations consequently assume sufficiently defined outgoing propagation velocities and neglect major subsequent changes during long-distance travel.

Temporal concentration modifies the rate at which electromagnetic energy reaches the observer; it does not itself generate the gamma-ray energy. For an ideal loss-free radiation beam, the integrated energy is conserved when the accounting is performed consistently in one observation frame. A separate transformation law is needed to compare energies attributed to the same radiation in the source and receiving frames. Likewise, high observed peak power does not by itself establish that the astronomical environment can supply the required total energy.

Different localized emitting regions may have distinct motions, energy supplies, and intrinsic spectra. Their contributions could therefore produce broader temporal components, spectral evolution, or delayed emission alongside the main gamma-ray maximum. These possibilities remain qualitative until a common dynamical and spectral model reproduces observed time lags, afterglows, fluences, and independent source associations.

The proposed interpretation remains open to decisive tests: independent evaluation of the propagation law in Part C2, quantitative verification of electromagnetic merging in Part B2, calculation of source-region kinematics and energy supply, and comparison with high-time-resolution, multi-band GRB observations. The main result is a conditional but explicit alternative timing mechanism: an observed gamma-ray burst could represent the concentrated arrival of electromagnetic energy emitted over a substantially longer period, rather than requiring an equally short intrinsic emission episode.

References

[1] Piran, T. (2004). The physics of gamma-ray bursts. *Reviews of Modern Physics*, 76(4), 1143–1210. https://doi.org/10.1103/RevModPhys.76.1143

[2] Kumar, P., & Zhang, B. (2015). The physics of gamma-ray bursts & relativistic jets. *Physics Reports*, 561, 1–109. https://doi.org/10.1016/j.physrep.2014.09.008

[3] von Kienlin, A., et al. (2020). The fourth Fermi-GBM gamma-ray burst catalog: A decade of data. *The Astrophysical Journal*, 893, 46. https://doi.org/10.3847/1538-4357/ab7a18

[4] Woosley, S. E., & Bloom, J. S. (2006). The supernova–gamma-ray burst connection. *Annual Review of Astronomy and Astrophysics*, 44, 507–556. https://doi.org/10.1146/annurev.astro.43.072103.150558

[5] Abbott, B. P., et al. (2017). Gravitational waves and gamma-rays from a binary neutron star merger: GW170817 and GRB 170817A. *The Astrophysical Journal Letters*, 848, L13. https://doi.org/10.3847/2041-8213/aa920c

[6] Goldreich, P., & Julian, W. H. (1969). Pulsar electrodynamics. *The Astrophysical Journal*, 157, 869–880.

[7] Spitkovsky, A. (2006). Time-dependent force-free pulsar magnetospheres: Axisymmetric and oblique rotators. *The Astrophysical Journal Letters*, 648, L51–L54. https://doi.org/10.1086/507518

[8] Karageorgopoulos, V., Gourgouliatos, K. N., & Contopoulos, I. (2019). Current closure through the neutron star crust. *Monthly Notices of the Royal Astronomical Society*, 487(3), 3333–3341. https://doi.org/10.1093/mnras/stz1507

[9] Blandford, R. D., & McKee, C. F. (1976). Fluid dynamics of relativistic blast waves. *Physics of Fluids*, 19, 1130–1138. https://doi.org/10.1063/1.861619

[10] Sari, R., Piran, T., & Narayan, R. (1998). Spectra and light curves of gamma-ray burst afterglows. *The Astrophysical Journal Letters*, 497, L17–L20. https://doi.org/10.1086/311269

[11] Nava, L., Ghirlanda, G., Ghisellini, G., & Celotti, A. (2011). Spectral properties of 438 GRBs detected by Fermi/GBM. *Astronomy & Astrophysics*, 530, A21. https://doi.org/10.1051/0004-6361/201016270